Intrinsic horizontal connections process global tactile features in the primary somatosensory cortex: neuroanatomical evidence

Journal:	*The Journal of Comparative Neurology*
Manuscript ID:	JCN-12-0344.R2
Wiley - Manuscript type:	Research Article
Keywords:	finger pad, primate, touch, tract tracing , optical imaging

SCHOLARONE™
Manuscripts

For Peer Review

Intrinsic horizontal connections process global tactile features in the primary somatosensory cortex: neuroanatomical evidence

László Négyessy[1,2], Emese Pálfi[1,2], Mária Ashaber[1,2], Cory Palmer[3], Balázs Jákli[4], Robert M. Friedman[5], Li M. Chen[6], Anna W. Roe[5]

[1]Department of Theory, Institute for Particle and Nuclear Physics, Wigner Research Centre for Physics, Hungarian Academy of Sciences, Budapest, H-1121 Hungary, [2]Department of Anatomy, Histology and Embryology, Semmelweis University Medical School, Budapest, H-1094 Hungary, [3]Department of Mathematics, University of Illinois, Urbana-Champaign, Urbana, IL 61801 USA, [4]Faculty of Information Technology, Pázmány Péter Catholic University, Budapest, H-1083 Hungary, [5]Department of Psychology, Vanderbilt University, Nashville, TN 37240-7817 USA, [6]Department of Radiology and Radiological Science, Institute of Imaging Science, Vanderbilt University, Nashville, TN 37203 USA

Running title: Cortical connections of fingertip representations

Associate Editor: Kathleen S. Rockland

Keywords: finger pad, optical imaging, primate, touch, tract tracing

Corresponding author: László Négyessy, Department of Theory, Institute for Particle and Nuclear Physics, Wigner Research Centre for Physics, Hungarian Academy of Sciences, P.O. Box 49, Budapest, H-1525, Hungary. E-mail: negyessy.laszlo@wigner.rmki.hu

For Peer Review

Funding. This study was supported by FIRCA NS059061 (to A.W.R. and L.N.), NS044375 (to A.W.R.) and the Hungarian Scientific Research Fund OTKA NN79366 (to L.N.).

For Peer Review

ABSTRACT

To understand manual tactile functions in primates it is essential to explore the interactions between the finger pad representations in somatosensory cortex. To this end, we used optical imaging and electrophysiological mapping to guide neuroanatomical tracer injections into distal digit tip representations of Brodmann area 3b in the squirrel monkey. Retrogradely labeled cell densities and anterogradely labeled fibers and terminal patches in somatosensory areas were plotted and quantified with respect to tangential distribution. Within area 3b, reciprocal patchy distribution of anterograde and retrograde labeling spanned the representation of the distal pad of multiple digits indicating strong cross-digit connectivity. Inter-areal connections revealed bundles of long-range fibers projecting anteroposteriorly, connecting area 3b with clusters of labeled neurons and terminal axon arborizations in area 1. Inter-areal linkage appeared to be largely confined to the representation of the injected finger. These findings provide the neuroanatomical basis for the interaction between distal finger pad representations observed by recent electrophysiological studies. We propose that intra-areal connectivity may be heavily involved in interdigit integration such as shape discrimination, while long-range inter-areal connections may subserve active touch in a digit-specific manner.

For Peer Review

INTRODUCTION

The hand and fingers, especially the distal pads, play fundamental roles in haptic exploration and tactile perception. Accordingly, the distal finger pads are distinguished by having one of the highest cutaneous receptor densities in the body (Weinstein, 1968; Vallbo and Johansson, 1984). To understand tactile perception it is crucial to identify the cerebral cortical mechanisms used to integrate information provided by the distal finger pads. Studies in human and non-human primates have identified areas 3b and 1 of primary somatosensory cortex (SI) as being crucial for tactile perception (LaMotte and Mountcastle, 1979; Bohlhalter et al., 2002; Kaas, 2004). SI is also well known for its topographic map of the body surface. Recent studies have found that neurons with receptive fields on the fingers in area 3b, the primary thalamocortical target of tactile information from the periphery (Shanks and Powell, 1981; Jones, 1983), are influenced not only by stimulation of adjacent skin areas, but also by stimulation of adjacent and non-adjacent fingers (Iwamura et al., 1983; Chen et al., 2003; Friedman et al., 2008; Reed et al., 2008, 2010a,b; Lipton et al., 2010; Thakur et al., 2012). This suggests that area 3b, in addition to area 1, plays a critical role in the spatial integration of tactile information originating from different distal finger pads.

Neuronal connections within and between the different somatosensory cortical areas, including area 3b and area 1, exhibit both a diffuse distribution and a patchy organization that could form the functional connectivity between neighboring finger representations (Krubitzer and Kaas, 1990; Burton and Fabri, 1995; Manger et al., 1997; Fang et al., 2002). However, previous anatomical studies are largely descriptive and have focused on examining large-scale neuronal connections between body parts and different somatosensory cortical areas. Burton and Fabri (1995) reported on connections between finger representations in the macaque after injections of anatomical tracers in areas 3b and 1. However, connections of distal finger pad

For Peer Review

representations have not been studied in detail. More specifically, whether cortical areas representing the fingertips are preferentially anatomically connected to other parts of the hand such as the representations of neighboring distal finger pads or to more proximal parts of the finger has not been explicitly examined. This question is fundamental to understanding the neural mechanisms of tactile perception. Answering such a question requires a detailed anatomical mapping of the connectional specificity in regard to the functionally identified cortical somatotopy in the different somatosensory cortical areas. Unlike in visual cortex (e.g. Ts'o and Gilbert, 1988; Malach et al., 1993; Levitt et al., 1994; Bosking et al., 1997; Kisvárday et al., 1997; Sincich and Blasdel, 2001; Ts'o et al., 2001; Buzás et al., 2006), this level of connectional precision has not been explored in the primate somatosensory cortex.

The goal of the present study is to identify, by way of bidirectional neuronal tract tracing combined with functional mapping, the input and target sites of the connections of distal finger pad representations in the somatosensory cortex of the squirrel monkey. Our studies focus on the intrinsic connections of area 3b and interareal connections of area 3b with neighboring area 1. The representation of the fingers in SI was mapped with optical imaging and electrophysiological methods; then one distal finger pad representation of area 3b was injected with neuronal tracers. Input and target preference of the site of tracer injection were defined first by mapping and calculating the densities of retrograde and anterograde labeling and second by aligning the two dimensional density maps with the functional maps obtained with optical imaging and neurophysiological recordings. Parts of this study have been published in abstract form (Négyessy et al., 2009; Pálfi et al., 2010).

MATERIALS AND METHODS

For Peer Review

Animal preparation

Two females (J, V) and one male (M) squirrel monkeys (0.8 to 1.1 kg) were used in this study. Each animal was sedated with ketamine hydrochloride (10 mg/kg) injected with atropine (0.05 mg/kg), intubated, placed in a stereotaxic frame, and mechanically ventilated with isoflurane for anesthesia (0.9–1.3%). Vital signs (blood oxygen saturation (SpO_2), heart rate, ECG, EEG, ET-CO_2, respiratory pattern, temperature) were monitored throughout an experiment. Body temperature was maintained between 37.0 - 38.5 ^{o}C via a circulating water blanket (Gaymar Industries, Orchard Park, NY, USA) and lactated ringers (with 2.5% dextrose) was infused intravenously (3ml/kg/hr) for hydration. After craniotomy (centered AP 6 mm and ML 15 mm) and durotomy, somatosensory cortex (area 3b and area 1) was exposed and identified by blood vessel landmarks. After tracer injection cortex was covered with artificial dura, the craniotomy closed and the skin sutured. The animal was then recovered from anesthesia and given appropriate analgesics. Repeated craniotomies and durotomies over the same area of cortex were separated by at least 10 days. All procedures were in compliance with and approved by the Institutional Animal Care and Use Committee of Vanderbilt University.

For Peer Review

Optical Imaging

Finger Stimulation. Topographic organization of digit-specific cortical activity was mapped by stimulating the glabrous skin of the distal, middle, and proximal finger pads with vibrotactile indentations (detailed descriptions in Chen et al., 2001, 2003; Friedman et al., 2004). Fingers were secured in plasticine leaving the glabrous surfaces available for tactile stimulation. Finger pads (D2-D4) were stimulated with a Teflon probe (2 mm diameter) mounted on a piezoceramic actuator (Noliac, Kvistgaard, Denmark) that was driven by a

Grass 88 stimulator (Grass-Telefactor, West Warwick, RI, USA). To optically map the cortical somatotopy of a finger pad, a stimulus consisted of a 3 sec train of 8 Hz square wave taps (pulse duration of 30 ms and indentation amplitude of 0.48 mm) was given. During the resting or blank condition, the probe was lightly touching the skin.

Image Acquisition. Images with 630 nm wavelength illumination were acquired through an optical chamber with a CCD camera using either a Redshirt Imaging System running CortiPlex software (Redshirt Imaging, Decatur, GA, USA) or an Imager 3001 system (Optical Imaging Inc., Germantown, NY). With the macroscopic tandem lens combination, the majority of the reflected light was derived from the upper 500 μm of cortex (Ratzlaff and Grinvald 1991). A blood-vessel map, used for landmark purposes, was collected with 570 nm illumination. Tactile stimuli were presented in a randomly interleaved manner in blocks typically consisting of 4 conditions (e.g. proximal, middle, distal sites on a single digit, and a blank no stimulus condition, or e.g. distal finger pads of D2, D3, D4 and blank). For each condition, 40-50 trials were collected. Intrinsic image maps were collected at 5 image frames per sec for 4 sec starting 200 msec prior to stimulus onset. Inter-stimulus intervals were between 8-10 sec.

Image Analysis. For each stimulus condition, image frames 6-15 were summed to maximize the signal-to-noise ratio. Deviation of this average from the first frame was calculated to generate an activation map. To reduce blood vessel artifact we used blank subtraction (where the 'blank' reference was a 3 second image acquired during no stimulus presentation, Blank condition). To delineate regions of strongest activation, images were low-passed filtered with a 10-pixel (150 μm radius) Gaussian spatial filter. To confirm reliability and consistency of the signal, we evaluated the frame-to-frame temporal development of optical images and

For Peer Review

compared the similarity of images obtained by summing different blocks of trials (Chen et al., 2001; Friedman et al., 2004).

Microelectrode electrophysiological mapping

The somatotopic and functional organization of the hand area has been well characterized in squirrel monkeys (Sur et al., 1982; Merzenich et al., 1987; Chen et al., 2001), and is important for interpreting the anatomical tracing results. Using the end of the central sulcus as the anatomical landmark, electrophysiological mapping, via insertion of tungsten microelectrodes into superficial cortical layers (depth 200-500 μm), was performed to specify the somatotopic organization of the hand region of SI (areas 3a, 3b and 1). The responsive skin area of the unit activity was identified by initially palpating areas on the contralateral hand while listening to the audio amplifier for spiking activity. In some instances thermal sensitivity was determined by placing a Peltier thermal probe on the skin and ramping up the temperature at 18 ^{o}C per sec from the 33 ^{o}C baseline temperature to a 3 sec duration plateau temperature of 49 ^{o}C.

Area 3b was typically found just anterior to the central sulcus, area 1 posterior to area 3b, and area 3a anterior to area 3b (Chen et al., 2001; Friedman et al., 2004, 2008; Sur et al., 1982). Area 3b was identified by single and multiunit response properties having small receptive fields (restricted to a single finger) and brisk responsiveness to light touch. In comparison to area 3b, area 1 units had larger receptive fields that often cover more than one finger. The cortical region between the representations of the distal finger pads in area 3b and 1 was marked by the representations of the middle phalanges and palm. The 3a/3b border was characterized by a tip-to-tip organization of the distal finger pads and a change in activation from cutaneous receptors in 3b to predominantly deep receptors that are activated by joint movement in 3a. Area 3a units often had large undefined receptive fields.

For Peer Review

In New World monkeys the existence of area 2 is still controversial (Kaas, 2004). However, until it is established that the squirrel monkey lacks area 2, in this study, we refer to the immediate region caudal to area 1 as area 2. We determined the approximate border between areas 1 and 2 by its tip-to-tip organization and the sharp reduction in responsiveness of area 2 to cutaneous stimuli, characteristic of area 2 under anesthesia (Pons et al., 1985; Pons and Kaas, 1986). Area 2 neurons often had large receptive fields that encompassed the entire hand. Because of the large receptive fields of neurons and the sensitivity to the stimulation of proprioceptors, the somatotopic organization of digits in areas 2 and 3a was less easy to define (Iwamura and Tanaka, 1978; Iwamura et al., 1993; Iwamura, 2000; Huffman and Krubitzer, 2001; Padberg et al., 2005). Thermal sensitive units were more commonly found in area 3a and occasionally in area 2 (Tommerdahl et al 1996; Chen et al 2009).

Demarcation of the areal borders and the digit representations with functional mapping

Both optical imaging and electrophysiological methods were used to delineate the somatotopic organization of the hand region of SI. Borders between cortical areas were estimated based on electrophysiological mapping, receptive field characteristics, and optical imaging. As we were concerned that a high density of electrode penetrations could obstruct the transport of tracers by accidental tissue damage, we performed a limited number of electrode penetrations: a detailed map was made in M (42 penetrations), only a few penetrations were used to identify the injection sites in V (n=4) and a moderate number of penetrations were made in J (n = 8). In case M and J, clear borders were placed based on optical imaging maps of the distal finger pads in areas 3b and 1; in case V, area 1 did not provide detectable optical signal during the experiment and the 3b/1 border was placed based primarily on area 3b activation. As has been observed in our previous studies, the optical

For Peer Review

imaging and electrophysiological maps were well matched (compare Figs. 1, 7 and 9) (e.g. Chen et al., 2001, 2003; Friedman et al., 2008).

Tracer Injection and Perfusion

In an effort to evaluate consistent features across cases, we focused on the connectivity patterns arising from injection of the distal digit 2 finger pad (D2t) representation in area 3b. In each animal the tracer injection was made in area 3b within the representation of the glabrous skin of D2t exhibiting a slowly adapting response to skin indentation. The targeted depth of the injection was 400 μm below the cortical surface (see Table 1 for measured depths). We used a 1:1 mixture of 10% biotinylated dextrans (BDA), BDA 10K and BDA 3K (final cc 5% each) (Molecular Probes, Eugene, OR, USA) dissolved in 0.01M phosphate buffer (PB, pH 7.4) and injected via iontophoresis (3 μA, 7 seconds on/off cycle) for 20 minutes. The combination of the two BDAs was used to trace both the input and the target connections of the injected cortical locus. It is known that in iontophoretic applications large MW BDAs including BDA10K is a more effective anterograde tracer, while BDA 3K is transported efficiently in the retrograde direction as well (Rockland and Knutson, 2000, 2001; Li et al., 2003). The tradeoffs of this strategy are described in the Discussion. In addition to the BDA injection all three animals received an iontophoretic injection of Phaseolus vulgaris leucoagglutinin (PhAL) (Vector Laboratories, Burlingame, CA, USA) into the D4t representation of area 3b. Visualization of BDA does not cross react with the PhAL labeling, as BDA histochemistry does not require immunohistochemical steps (see below). The present study is focused on the BDA labeling, the PhAL labeling was described elsewhere (Pálfi et al., 2010).

After a survival period of 10-20 days (J: 10 days, M: 14 days, V: 20 days), transcardial perfusion was initiated under a deep level of anesthesia with phosphate buffered

For Peer Review

saline (PBS), followed by a 40 minutes perfusion with 1 liter of fixative consisting of 4% paraformaldehyde, 0.1% glutaraldehyde and 0.2% picric acid in 0.1M PB (pH 7.4). A block of cortex containing areas 3b, 1, 2 and 3a was then cut from the brain, flattened and postfixed in 0.1M PB (pH 7.4) containing 4% paraformaldehyde at 4 ^{o}C.

Tissue processing

Series of 50 µm thick horizontal, vibratome sections were collected at 130 (V, J) and 270 (M) µm spacing. Before collecting the series, the flattened cortex was approached by the vibratome blade with 100 µm steps. The three topmost sections collected contained arachnoidal tissue and the 3rd included the very surface of neural tissue with patterns of blood vessels running parallel to the cortical surface similar to the previous 2 sections. We began collecting the 50 µm thick series after the 3rd superficial sections. In the reconstructed series, horizontal vessels changed directions and become penetrating vessels as represented by the cross sections of blood vessels (Fig. 2).

The standard ABC (Elite kit, Vector Laboratories, Inc. Burlingame, CA, USA) protocol was used to visualize BDA labeling with nickel intensified diaminobenzidin (NiDAB) (Sigma-Aldrich Kft, Budapest, Hungary) as the chromogen (for more details about the procedure see Négyessy et al., 2000). In short, sections were incubated in ABC (1:200 in PB, 0.1M, pH 7.4) overnight at 4 ^{o}C after freezing-thawing of the cryoprotected sections (30% sucrose in PB), reducing unbound aldehydes with borohydride (1% $NaBH_4$ in PB, 30 min) and blocking intrinsic peroxidase activity by 1% H_2O_2 in PB, 30 min. After the NiDAB reaction sections were osmicated (1% OsO_4 (Electron Microscopy Sciences, Hatfield, PA, USA) and 5% sucrose in PB for 60 minutes), dehydrated, infiltrated with resin (Durcupan, Sigma-Aldrich Kft, Budapest, Hungary) and flat embedded on coated glass slides (liquid release agent, (Electron Microscopy Sciences, Hatfield, PA, USA).

For Peer Review

Analysis of the retrograde and anterograde BDA labeling

Maps of the BDA label were generated using Neurolucida® (MicroBrightField Europe, E.K. Magdeburg, Germany) and an Olympus research microscope equipped with a motorized stage (MultiControl 2000, Märzhäuser Wetzlar GmbH & Co. KG, Wetzlar, Germany). Retrogradely labeled cell bodies were mapped at 10x and 20x (objective magnification) while axonal fibers (anterograde labeling) were reconstructed at 20x and 40x. Terminal patches (see Results) were examined at 10x and 20x and outlined individually on each section. The size of the individual patches was measured by Neurolucida Explorer using the Feret maximum and Feret minimum functions (Negyessy and Goldman-Rakic, 2005). A Feret diameter is a width of the closed contour as if measured with calipers. For a terminal patch, the Feret minimum was the shortest diameter of the closed contour and the Feret maximum was the largest diameter. The average of the Feret maximum and minimum was calculated for the comparative analysis.

Quantitative analysis of the density distribution of bouton-like structures is a highly valuable method for revealing the functional specificity of cortical connections (Kisvárday et al., 1997; Buzás et al., 2006). These studies count the total number of bouton-like structures along local, horizontal connections. However, this approach is not feasible for large areas such of those studied here; so instead we counted bouton-like structures in selected regions, which represented either potential target sites or were devoid of BDA labeling.

Densities of axon terminal-like structures were measured in regions containing either terminal patches, tracks of long range axons, or selected regions lacking retrograde labeling or distinct anterograde labeling. Each defined region was sampled in 3 neighboring 50 μm^2 rectangles (i.e. 150 μm^2) with a 100x objective in the full depth. Except for regions lacking BDA labeling, the sampled areas were placed in a way to avoid the inclusion of vessels,

For Peer Review

perikarya and dendritic processes in the overlapping part of the patches on the consecutive sections. Selected regions were localized in all areas including areas 3b, 3a, 1 and/or 2. Altogether in the three cases 18624 bouton-like structures were counted in 49 regions (18 terminal patches, 16 fibers of passage, 15 without retrograde labeling). To obtain baseline measures, almost twice the numbers of sampled areas were outside of terminal patch regions. Mean bouton densities and standard deviations were computed and compared for different regions and areas.

Density measurements of the retrograde labeling of cell bodies were performed by applying a Voronoi tessellation algorithm (for a short overview see http://mathworld.wolfram.com/VoronoiDiagram.html or http://en.wikipedia.org/wiki/Voronoi_diagram), with software written in-house in the Python programming language, after collapsing the serial reconstructions into a single two dimensional representation. Voronoi tessellation generates equidistant segment lines between nearest neighbors' points, or in our case retrogradely filled neurons. Connecting the endpoints of the equidistant segment lines between the nearest neighbors define an area around the points, which is used as a measure of density. Thus, Voronoi areas are inversely related to the density of the BDA labeled neurons. To compare across cases, the two dimensional density plots were standardized by computing how many standard deviations an individual Voronoi density area, after performing a logarithmic transformation, departed from the mean Voronoi area. For display, the standardized density values were either grayscaled or color-coded within a range of 3 units of standard deviation (SD) above and below the average Voronoi area. Labeling around the core of the injection site, that measured 250-300 μm diameter, was omitted from the analyses, and the distance between the serial sections was ignored.

For Peer Review

Images of the BDA labeled structures were obtained by a digital camera (Olympus DP50) mounted on an Olympus BX51 microscope. Contrast and brightness were adjusted and photos were mounted on figures in Adobe Photoshop (Adobe Systems Inc., USA).

Alignment procedures

Sections were scanned with software written in-house with a 4x objective mounted on the microscope used for the Neurolucida reconstruction. In Photoshop, the three topmost sections were aligned with an image of the cortical surface based on the horizontal pattern of the blood vessels. Scanned images of the 50 μm thick series of the consecutive sections were then aligned with the topmost sections and to each other by using blood vessel patterns and cut edges of the sections (Fig. 2). Reconstruction of the BDA labeled structures was made by using the serial section reconstruction function of Neurolucida, which results in a complete alignement of the series of drawings. Finally, the Neurolucida drawings were aligned with their corresponding scanned sections which resulted in the alignment of the serial reconstruction with the cortical surface.

For Peer Review

RESULTS

Alignment of optical images, electrophysiological maps, and anatomical reconstructions and defining borders

To identify locations of digit maps in areas 3b and 1, optical imaging and electrophysiological mapping methods were used (e.g. Chen et al., 2001, 2003; Friedman et al., 2008). In each case optical maps of 3-4 digits were obtained. This revealed the lateral-to-medial cortical representation of D2, D3 and D4. These mapping procedures were also useful

for determining areal borders as shown in Figure 1 where activations were obtained following vibrotactile stimulation of proximal (A), middle (B), and distal (C) phalanges of D4 (in case M). These maps revealed activation along the areas 3b/1 border (A), just anterior and just posterior to the areas 3b/1 border (B), and further anterior and further posterior to the areas 3b/1 border (C), consistent with the distal-to-proximal mapping along digits within areas 3b and 1. This pattern of activation was characteristic of imaged digit maps in areas 3b and 1 of the squirrel monkey and provided an approximate placement of the areas 3b/1 border (dotted red line in A-C).

Subsequent to optical imaging, electrophysiological mapping surrounding digit activation sites were conducted (Fig. 1D). This served not only to confirm optical maps, but also to evaluate areal identity and border location based on functional response type and receptive field sizes. In the map shown in Figure 1D, receptive fields in areas 3b and 1 exhibited clear topographic progression and had brisk sustained or phasic responses to tactile stimulation. A primary difference between areas 3b and 1 was receptive field size: receptive fields of units recorded in area 3b were small and confined to single digits while those in area 1 were larger, at times spanning 2 or 3 digits (cf. Friedman et al., 2008). The border region between areas 3b and 1 comprised a greater number of sites with palmar receptive fields while those at the area 3b/3a border were largely located on digit tips (D2t, D3t and D4t). Units in area 3a were difficult to drive with tactile stimulation and were often activated only by sustained, deep stimulation and joint movement, consistent with deep receptor activation previously described for area 3a (Huffman and Krubitzer, 2001; Krubitzer et al., 2004). Some units in area 3a were also activated by thermal stimulation as previously described (Tommerdahl et al., 1996). The border between area 1 and area 2 was often difficult to place with confidence. We typically found units in area 2 had large receptive fields (e.g. some spanning D2 base/join, D3 palm/deep, D2 palm cutaneous), were noticeably more difficult to

For Peer Review

drive, had more mixed responses (e.g. some heat responses, some deep responses), and were characterized by palmar receptive fields. Thus, we were reasonably confident about the borders between areas 3a and 3b as well as between areas 3b and 1, and less certain about the borders between areas 3a and presumed Brodmann area 4 (M1) as well as that of area 1 and area 2. Injections were then placed at selected sites in area 3b. In the case shown in Figure 1, the injection of BDA was made at the location of the D2 tip.

An example of the precision of alignment was shown in Figure 2 for the optical maps (Fig. 2B,C), electrophysiological maps (Fig. 2A), the tracer injection (Fig. 2D,E,G) and transported tracer location (Fig. 2F,G) maps. This was done by carefully aligning imaged vessel maps (Fig. 2A) with histological sections, using sections at the surface which contained evident vessel patterns (cf. Kaskan et al., 2009), and by aligning blood vessel lumen with locations where vasculature enters cortex at the surface (see corresponding circled locations in Fig. 2D and E enlarged on G). As this region of squirrel monkey cortex is fairly flat, tissue distortion was minimal. Alignment was based on blood vessel landmarks (open circles in Fig. 2), electrode penetrations (colored dots in Fig. 2A,F), optical activations (white arrows in Fig. 2C) and injection site (blue arrow in Fig. 2A). Alignment between blood vessel landmarks in the brain and vessel lumen in the histological tissue (compare open circles in Fig. 2A and E) permitted precise alignment between the functional maps (Fig. 2C) and the anatomical label (Fig. 2F). Distant to the injection site alignment of landmarks was not as good. Altogether, the alignments resulted in single composite maps containing identified digit maps, distribution of labeled cells, and distribution of labeled fibers and terminal axon arborizations.

BDA injections and morphological appearance of the labeled structures

In all three cases injections were successfully localized to the middle and supragranular layers and were confined to within a single digit tip representation (Fig. 3,

For Peer Review

Table 1). Injection cores were approximately 300 μm, well within the 1 mm size of single digit activations (Figs. 3, 4, Table 1). As shown in the sections taken from a supragranular layer, the size and location of the injection sites were similar; however, there were some noticeable differences in the different cases (Fig. 4). Injection sites in J (Fig. 4B) and M (Fig. 4C) with 10 and 14 day survival times, respectively, were characterized by a core region of about 250-300 μm diameter surrounded by a halo made up by a very dense plexus of neuronal processes. Both regions included BDA-labeled perikarya. In case V core and halo regions were less dense due to the longer, 20 days survival time (Fig. 4A).

BDA injections also revealed multiple dense spots of label that were found up to several millimeters away from the injection site (Fig. 2D,E,G). These spots fell within areas 3b, 1, 3a (and presumed M1 and area 2). These distributions were quantified and will be presented in later figures.

Retrograde labeling of cell bodies and dendrites. In all three cases retrograde BDA labeling of neuronal perikarya were observed in cortical regions near to and distant from the injection site (e.g. Figs. 2, 4). Except for a few smooth dendritic neurons near the injection site, retrogradely labeled neurons were identified as pyramidal cells on the basis of their frequently branching dendrites decorated by numerous spines (Fig. 5A,B) and an apical dendrite, which could be identified by changing the depth of focus of the microscope. The smooth dendritic neurons were distinguished by a relatively large soma and the lack of spines on the varicose dendrites, which were thin and gave birth to a relatively few branches. Due to the low number of the BDA labeled smooth dendritic neurons, these cells were not studied further.

Anterograde labeling of axons and axonal arborizations. Intense anterograde labeling revealed the fine details of axons (Fig. 5B-F). Three different kinds of anterograde labeling

For Peer Review

were distinguished with Figure 5E,F showing examples of long axonal segments emanating from an injection site. 1. BDA labeled relatively thick, smooth axonal processes lacking bouton-like structures (Fig. 5E). 2. Relatively thick, horizontally (i.e. parallel to the cortical layers) oriented long-range fibers containing bouton-like structures were commonly observed. Bouton-like structures were identified both as boutons with stalk (Fig. 5F) and varicosities (Fig. 5B,F).

The third type, patches of terminal-like axon arborizations contained a dense meshwork of thin fibers with numerous bouton-like enlargements in a relatively well-circumscribed location on individual sections (Fig. 5C,D). Terminal patches were of special interest as these are target zones of the injected cortical locus and their clustering on the serial reconstructions indicates a preferred target area. After manual demarcation of the terminal patches (Fig. 5C, pale contour), the network of thin fibers and bouton-like structures were examined at high magnification (Fig. 5D). Fine axonal processes were distinguished from spiny dendrites by size, type of protrusions, and the more tortuous appearance (compare Fig. 5D with Fig. 5B).

Overall distribution of retrograde and anterograde labeling

Retrograde labeling. Examination of the tangential distribution of the retrograde labeling (black triangles in Fig. 6A-C, tessellation density maps on Fig. 6D-F) revealed a similar pattern in all three cases. Heavy labeling was observed in an area of 1 to 2 mm diameter (cases J, M and V, respectively) around the injection site (Fig. 6A-F). Although, outside of this region labeling density dropped with distance, clusters of retrogradely labeled neurons appeared medially, laterally as well as caudally to the most heavily labeled region within area 3b (Fig 6A-F). Outside of area 3b retrogradely labeled neurons formed dense clusters in areas localized both rostrally and caudally to area 3b (Fig. 6A-F). We suspect that survival time was

For Peer Review

a factor only in the numerosity/amount of labeling since in V (20 days post injection) more neurons were labeled when compared to that of J and M (post injection days 10 and 14, respectively). In J and M the number of BDA labeled neurons did not considerably differ.

Anterograde labeling. A similar distributional pattern of anterograde BDA transport appeared in all the three cases (Fig 6G-I). Survival time affected anterograde labeling more than retrograde (Fig. 6). Survival time was critical for the labeling of terminal patches (green ovals, Fig. 6G-I). Case J had the shortest transport period (10 days) resulting in only a few terminal patches. Case M had an intermediate transport period (14 days) resulting in intermediate number of patches, whereas case V had the longest transport period (20 days) and the largest number of the terminal patches. BDA-labeled long range fibers were abundant in all three cases (curved lines). In cases M and J long-range fibers were traced from the core of the injection site; but interestingly, long-range horizontal axonal fibers appeared mostly at a distance from the injection site in V. Case M, which had 14 days survival after the injection, exhibited an intermediate pattern of anterograde labeling characterized by numerous terminal patches and horizontal fibers originating close to the injection site.

Unmyelinated axons decorated with bouton-like enlargements and thick and smooth fibers lacking bouton-like structures were observed projecting in all directions (Fig. 5B,E,F). Some of these smooth and thick horizontal axons could have represented myelinated fibers. In the deep layers, where axons turned into a perpendicular direction while leaving and/or entering the gray matter, cross sections of BDA-labeled myelinated fibers were identified by the ring shaped osmium stained myelin sheath encapsulating NiDAB stained axonal process (not shown). Many of the long range smooth and thick horizontal fibers were found projecting caudally from the injection site, apparently toward areas 1 and/or 2. Since the techniques used in this study did not allow the unequivocal identification of myelinated fibers, the question

For Peer Review

whether connections of area 3b with areas 1 and 2 were composed by a significant proportion of myelinated axons remains to be clarified.

Similar to the patterns observed from retrograde labeling, the horizontal connections appeared to project in two major directions: mediolateral and rostrocaudal (Fig. 6, blue and red lines, respectively). Terminal-like arborizations (i.e. patches) (except in case J, which had short survival times) were localized near the termination of the long-range fiber tracks; this pattern was most evident in M (Fig. 6I). Overall, despite differences in the amount of anterograde labeling a similar distributional pattern of anterograde BDA transport appeared in all the three cases, which was characterized by a distinct mediolateral and a rostrocaudal orientation of the labeled fibers and terminal patches.

Reciprocity. The overlapping characteristic of anterograde and retrograde labeling was clearly detected after aligning the terminal patch distribution with the density maps of retrograde label (Fig. 7). Retrogradely labeled neurons were clustered in regions with terminal patches and/or around the target zones of BDA-labeled long-range axonal fibers. The distribution of the highest density of retrograde labeling was in a good correspondence with the distributional pattern of the terminal patches; otherwise, the low density retrograde labeling overlapped with the course of long range axonal fibers.

Terminal axon arborizations: characterization of the major target sites

We measured the size of terminal patches by averaging the minimum and maximum width of each patch (Feret measurements). The diameter of the terminal patches varied around 200-300 μm (Fig. 8A) within areas 3a, 3b, and 1. This was consistent with the size of functional domains (preference for pressure, flutter, or vibration) observed previously by optical imaging in the squirrel monkey SI (Friedman et al., 2004) and with patch size

For Peer Review

observed in the visual cortex (e.g. Sincich and Blasdel, 2001). For all cases, the size of the patches did not differ statistically between areas ($P > 0.05$).

To quantify whether terminal axon arborizations originating from a distal finger pad representation of area 3b have a higher probability of forming synaptic connections with other regions of SI, the density of axon terminal-like structures were compared in selected locations. The mean number and standard deviation of bouton-like structures in regions containing patches of terminal like axon arborizations (P), in regions containing fiber tracts (F), and in regions devoid of BDA labeled axonal tracks and cell bodies (CF) were measured as shown in Figure 8B after combining the data from the individual cases. Consistent with our qualitative observations, regions containing patches of terminal like axon arborizations (P) showed a greater number of bouton-like structures than regions containing only fiber tracts (F) or devoid of labeled fiber bundles and cell bodies (CF). This observation was verified by statistical comparisons for the individual cases (Table 2). One exception was V, where density differences of the bouton-like structures did not reach statistical significance between the terminal patch (P) and fiber tract (F) regions (Table 2). Terminal patch regions (P) of all areas examined (areas 3b, 1 and/or 2, and 3a) exhibited similar densities of bouton-like structures for each of the three cases. Considering reciprocity, it was also interesting to note that regions of low density retrograde labeling consisting of fiber tract regions (F) and regions devoid of labeled fiber bundles and cell bodies (CF) exhibited a low density of bouton-like structures (Fig. 8B); within these regions the density of bouton-like structures was not statistically different in the individual cases (Table 2). Therefore, the density of bouton-like structures, which suggest a high probability of synaptic contact, supported the assumption that terminal patches represent the preferential target regions of the injected cortical regions.

For Peer Review

Overlaying anatomical and functional maps: input and target preferences of the connections of distal finger pad representations

To relate the total distribution of cells and terminal patches to the functional maps, we aligned and projected the serial reconstructions to the cortical surface in each of the three animals (see Figs. 1, 2).

Intrinsic connections of area 3b. The highest density of retrograde labeling (1-3 SD above average) was localized to the injected distal finger pad representation in all three cases (Fig. 9A-C) with the exception of case V (Fig. 9A), where the highest density labeling spread into neighboring regions medial and caudal to the representation of D2t. Interestingly, while retrograde density decreased away from the D2t representation, high labeling density was still present in the D3t region. In contrast, the density of label was in general 2-3 SD higher in the D3t region than in the representation of D4t region. Lateral to the injected D2t representation a similar high labeling density was found in the region corresponding to the D1t representation, which was clearly shown in case V and could be inferred on the basis of the consistency of the labeling pattern and the known topography in the other two cases (Fig. 9A-C). Notably, in the region corresponding to the D1t representation labeling density was higher than that found in the D4t region. In addition to the mediolateral distributional pattern, high density labeling was also present caudal to the D2t region representing most probably the more proximal parts of D2 (Fig. 7, 9A-C).

Terminal axon arborizations could not be distinguished in the BDA uptake zone. Accordingly, within the injected fingertip region, patches were localized near the border of the D2 tip outlines on the overlain anatomical and OIS maps in all 3 cases (Fig. 9D-F). Some of these target regions of D2t were clustered over locations where D2t and D3t representations overlapped as in cases J and M (Fig 9E,F). In case V (Fig 9D), which had the

For Peer Review

most abundant anterograde labeling, terminal patches were localized in the representation of D3t and D1t. The non-adjacent D4t region was devoid of terminal axon arborizations in all the ceases studied. In case V (Fig. 9D), similar to the retrograde labeling terminal patches outside of the distal finger pad representation also appeared more caudally to include the representation of the presumed proximal parts of the injected finger (Fig. 9D-F).

The reciprocal pattern of retrograde and anterograde labeling described above was consistent across the different cases (Fig. 7, 9). Regions of low density retrograde labeling were also regions with few terminal patches. As in case J (Fig 9B,E), the caudal region including most probably the palm and proximal finger representation regions (near the border of areas 3b and 1) were regions of low cell density and were devoid of patches of terminal axon arborizations. Regions of lower density retrograde labeling were also regions through which intrinsic horizontal fibers radiate from the injection site. Thus, within area 3b, labeling was concentrated in the location of the injected digit and extended to nearby digit representations.

Connections with other areas of somatosensory cortex. Inter-areal connections appeared more focused than the intrinsic connections of area 3b (Fig. 7, 9). In area 1 the highest density retrograde and anterograde labeling was restricted to the homologous and nearby distal finger pad representations. This was evident in cases J and M, where the topography of fingers could be mapped (Fig. 7, 9). Somewhat surprising, in case M peak density of retrograde labeling as well as terminal patches were localized primarily in the distal finger pad representation of D3 in area 1. However, in M injection of BDA was delivered into a D2t region of area 3b, which overlapped with that of D3t (Figs. 3F, 7C, 9F). Similarly, in J (Fig. 9J) a few terminal patches appeared in the D3 tip region of area 1 ; however, the vast majority of terminal axon arborizations were localized to the D2t representation. In case V, similar to cases J and M, the

For Peer Review

highest density of labeling was localized within a mediolaterally restricted region caudal to area 3b, which suggests a homotopic connectivity of area 3b with area 1 in this case as well (Fig. 9D).

In addition to the labeling in area 1, two other concentrations of labeling were detected in regions rostral to area 3b: one close to the border of the injected area and another in a more distant rostral area (Fig. 9). In case V this pattern of rostral labeling was apparent in both the retrograde and anterograde labeling. A similar pattern emerged in case M except that the most rostral peak density of retrograde labeling was not reciprocated by terminal patches. In case J only the retrograde labeling exhibited a clustered rostral labeling pattern. Based on the electrophysiological recording in M, the rostral region of label in the vicinity of area 3b could be identified as area 3a (Fig. 7). On the other hand, the more distant region was presumably localized within M1 on the basis of the organization of sensorimotor cortex (Fig. 7, 9). The highly restricted localization of labeling within these rostral areas suggested a similar focal localization of connections with respect to the finger representation as found in area 1. Finally, similar to intrinsic connections, inter-areal connections of area 3b were organized reciprocally (Fig. 7, 9).

For Peer Review

DISCUSSION

Overview

Our results were in good agreement with findings of previous studies using different neuronal tracers and injection protocols (Krubitzer and Kaas, 1990; Burton and Fabri, 1995; Manger et al., 1997; Fang et al., 2002). However, previous tracing studies used bulk labeling and qualitative analyses of the distribution of the labeled neuronal elements. In the present

study, we used both optical imaging and electrophysiological maps to guide tracer injections and to interpret the functional locations of transported label. Notably, in the present study the injection sites were restricted to single digit tip representations. This permitted the exploration of the finer details required to define the connectional relationships of the distal digit pad representations. Such scale of anatomical and functional alignment had not previously been conducted.

We find both intra-areal and inter-areal connections are connected reciprocally, as patches of dense axonal ramifications overlap areas with high density of retrograde labeling. By careful alignment of electrophysiological maps with the neuronal tract tracings, this study has provided the first direct evidence that in area 3b representations of neighboring distal fingers are preferentially connected to each other. Connections are strongest between adjacent fingertip representations but also extend to non-adjacent digit representations. This results in a mediolateral axis of label distribution. In contrast, extrinsic connections of area 3b with neighboring somatosensory cortices, especially for area 1, appear focal and could have been mostly restricted to homotopic representations of the injected regions (e.g. D2t to D2t). Thus these connections are mediolaterally restricted in extent, and result in an antero-posterior axis of label distribution. Overall, this pattern produces a visually striking neuroanatomical orthogonality of intra-areal (mediolateral orientation) vs. inter-areal (antero-posterior) integration. Accordingly, the findings suggest that intrinsic connections of area 3b subserve global tactile functions by integrating information from multiple digits. On the other hand, connections of area 3b with other cortical areas are more strongly confined to convey digit-specific information (see discussion below).

Methodological considerations

For Peer Review

Bidirectional tracing. The combination of low and high molecular weight BDAs is a recommended bidirectional neuronal tracing method in the primate cerebral cortex (Rockland and Knutson, 2000, 2001; Li et al., 2003). A possible disadvantage of bidirectional tracing is that it could backfill axons emanating from retrogradely labeled neurons located distal from the injection site. This would result in the appearance of "secondary" target areas of the injected cortical locus via the retrograde labeling. Although we cannot exclude this possibility (as full reconstruction of neurons was not possible in our regularly spaced series), some observations suggest that this phenomenon was negligible in our cases. First, we find that reconstructed axons ramified usually toward the distant terminal patches suggesting an outward direction of these axons from the injection site. Second and most significantly, we observe that terminal patches accumulated in regions that had a high density of retrograde labeling, while, assuming divergent neuronal connectivity, axonal backfilling would have resulted in the appearance of terminal axon arborizations in regions without significant retrograde labeling.

Other methodological considerations that could have influenced our results include post injection survival time and experimental differences that can occur during the injection. As addressed in the Results section, longer survival times are critical for a sufficiently strong labeling of the terminal patches. Compared to BDA 3K, BDA10K is a more selective anterograde tracer (Rockland and Knutson, 2000) and its neuronal transport is slower, which could explain the sensitivity of anterograde labeling to the survival time. Another notable factor is the variation of the size of the glass capillaries used for the tracer injections. Thicker capillaries could result in the leakage of more tracers, which in turn would result in more retrogradely and anterogradely labeled structures. Any minor tissue damage caused by the electrode penetrations during the initial electrophysiological mappings might also influence the transport of BDA. However, the consistent pattern of labeling across cases make these

For Peer Review

issues less of a concern, and increases our confidence in the results. Furthermore our quantitative approach (including normalization) proves its usefulness as it was robust against the variability of the amount and spatial spread of the labeling inherent in all kinds of tract tracing studies.

Precision of the functional mapping and the alignment. Another important methodological consideration, as detailed in the Materials and Methods section, was that complete, highly detailed functional maps were not acquired; therefore, borders between cortical areas and finger representations had to be inferred. However, the complementary data obtained from the three cases allowed us to make firm conclusions in regard to the specificity of the connectional patterns observed.

Regarding the precision of our alignment, we should note that throughout our procedures there are many potential sources of distortion including photo optical (spherical aberration), histological, as well as the reconstruction methods, all of which can lead to imperfections in alignment. It is also important to note, that compared to similar studies on the visual cortex (e.g. Ts'o and Gilbert, 1988; Malach et al., 1993; Levitt et al., 1994; Bosking et al., 1997; Kisvárday et al., 1997; Sincich and Blasdel, 2001; Ts'o et al., 2001; Buzás et al., 2006), we used relatively large sections, which makes alignment even more difficult. However, our alignment procedures resulted in the highest precision, and we are especially confident of alignment in regions around the injection site in area 3b. The scattering observed in the alignment distant from the injection site does not fundamentally alter our findings.

Patchy anterograde labeling in somatosensory cortex

Other studies have revealed a patchy organization of terminal-like labeling in somatosensory cortex (Krubitzer and Kaas, 1990; Lund et al., 1993; Manger et al., 1997).

For Peer Review

Lund et al. (1993) noted that patchy organization of the anterograde labeling was less obvious in somatosensory than visual cortex. In the present study terminal patches was clearly observed. However labeling density within the patches varied; consequently, patches of lower density labeling were hard to unequivocally outline and other patches could have been missed. Nonetheless, delineating dense patches were straightforward. The size of the patches identified in this study was very similar to that described by others (Lund et al., 1993; Sincich and Blasdel, 2001). The terminal patches also exhibited a similar size (200-300 μm) to the functional domains described in previous studies (Chen et al., 2001; Friedman et al., 2004).

Among the possible target regions only terminal-like axon arborizations exhibited high densities of bouton-like structures. This analysis provided quantitative evidence that terminal patches represent the specific target sites of the distal finger pad representation in primary somatosensory cortex. Moreover, our results suggested that connections, both intrinsic and long range, between different somatosensory cortical regions are reciprocal, which was most evident in terminal patches. However, a low density distribution of bouton-like structures was also observed in regions of low density retrograde labeling in all areas studied. This scattered labeling spread throughout area 3b and also included much of the neighboring areas permitting widespread potentially subthreshold interactions within the pre- and postcentral gyri. Such pattern of connectivity could form the neuroanatomical basis of unmasking following deafferentation (e.g. Calford, 2002).

New views of functional integration in the hand representations of area 3b and area 1

Intra-areal connectivity. The prevailing view of area 3b organization is that the response properties of cells are relatively simple, with receptive fields confined to single digits (e.g. Sur et al., 1985; DiCarlo et al., 1998). Contrary to this idea, recent electrophysiological studies reveal significant inter-digit integration across fingers within area 3b (Reed et al., 2008,

For Peer Review

2010a,b; Lipton et al., 2010). Furthermore, study of suppressive surrounds suggests that the heaviest interactions occur between neighboring fingertip regions digits (Thakur et al., 2012). Similarly, optical imaging and fMRI studies of the tactile funneling illusion showed that stimulation of multiple digit tips leads to a single site of cortical activation in area 3b, which provides evidence for a functional significance of interdigit integration in area 3b (Chen et al., 2003, 2007). Such interdigit integration may also exist in other cortical areas, as similar observations have been made in area 1 (Friedman et al., 2008; Ashaber et al., 2011). In agreement with these electrophysiological and imaging observations, the present neuroanatomical findings indicate that there is strong connectivity between the representations of distal finger pads of area 3b (cf. Krubitzer and Kaas, 1990; Burton and Fabri, 1995; Manger et al., 1997; Fang et al., 2002). Further studies are needed to clarify the complex cortical neuronal circuitries subserving multi-digit integration. Nevertheless, these findings indicate that integration of cross-digit tactile information begins as early as area 3b. We suggest that intra-areal connections in area 3b play prominently in shaping multi-digit representation of global features of tactile objects, transfer of tactile aftereffects between fingers (Kappers, 2011), and in multifinger tasks and haptic exploration (Dijkerman and de Haan, 2007).

Inter-areal connectivity. With respect to inter-areal relationships, this study also shapes existing views. Based on the evidence that area 1 receives the bulk of its ascending input from area 3b (Shanks and Powell, 1981; Jones, 1983) and that ablation of area 3b silences area 1 (Garraghty et al., 1990), traditional views have suggested a hierarchical relationship between areas 3b and 1 (e.g. Powell and Mountcastle 1959; Sur et al., 1985). In contrast to small receptive fields in area 3b, area 1 neurons integrate information over larger skin areas and have higher order response properties such as preference for texture, roughness, or motion

For Peer Review

(Bensmaia et al., 2008; Pei et al., 2010; Tremblay et al., 1996). Accordingly, it is assumed that convergence of afferents of area 1 originating from area 3b is responsible for the observed somatosensory cortical hierarchy (Iwamura, 1998). It is true that receptive fields in area 1 are larger and can span more than a single digit. However, it has been observed that the receptive fields of neurons within a single (600 μm) column of cortex in area 1 vary in size and shape. Importantly, they all share a single small area (hotspot) on the skin (Favorov and Whitsel 1988). Thus, when the population response is examined as in 2-deoxyglucose (Tommerdahl et al 1993) or optical imaging studies (Chen et al 2003, Friedman et al 2008), a small focal activation spot is revealed when single digit tips are stimulated. Our anatomical data provide further context to these observations. That is, we suggest that the variability in size and shape of receptive fields in area 1 may be contributed largely by intra-areal connections (Ashaber et al 2011) whereas the focal hotspot of activity is maintained by inter-areal connections. Thus, our concept of single digit representation in area 1 is captured by the term hotspot. Maintaining such a hotspot could be consistent with maintaining a relatively low level of divergence from area 3b to 1. These data thus shed light on how somatotopic maps emerge and diverge from one cortical area to the next (Sur et al., 1980).

Functional Implications

Motion processing circuitry in SI. Within area 1 neuronal responses are invariant to the specific cues contributing to the perception of motion supporting the view that it is a 'motion processing' area and consistent with the predominance of cells with rapidly-adapting responses (Pei et al., 2010). In contrast, neurons selective for orientation tend to be slowly-adapting, a response type more common in area 3b than area 1 (Bensmaia et al., 2008). The findings of this study further refine this view by heavily restricting the interaction between areas 3b and 1 to homologous digit tip representations, or potentially more generally to

For Peer Review

homologous skin representations. Thus, in contrast to the multi-digit integration present in area 3b, the functional transformations between areas 3b and 1 in the hand region are more digit-specific and, moreover, are focused mostly to the fingertips. Interactions within and between visual cortical areas could help understanding how the somatosensory cortical circuitry described here is operating. As reviewed by Gilbert et al. (2009), activation of long range, intrinsic horizontal connectivity of V1 gated by top-down effects via inputs from higher order areas play a part in the neurobiological mechanisms of perceptual learning and plasticity. Activity of intrinsic horizontal connections of area 3b interacting with area 1 could subserve similar functions.

Braille reading. There are many studies on the use dependent plasticity of the somatosensory cortical representation (for reviews see Jones et al., 2000; Godde et al., 2003; Wolters et al., 2005; Fox et al., 2009). In one example, blind subjects that use a single finger to read Braille have an expanded somatosensory cortical representation of that finger (Sathian and Stilla, 2010). Alternatively, the use of multiple fingers to read Braille can result in a disordered cortical representation accompanied by a reduced ability to localize finger stimulation (Sterr et al., 1998). Our findings suggest that existing intra-areal connectivity of area 3b provides at least in part a neuroanatomical locus of such use dependent plasticity. Most notably, in multiple-finger Braille readers a strengthening in the connectivity between the finger representations of area 3b could account for the decline in spatial discrimination. Considering further cortical processing, the spatial integration of tactile information in area 3b along with finger specific inter-areal connections described here could transmit multiple finger information in a finger independent manner throughout somatosensory and perhaps motor cortical system as well.

For Peer Review

Acknowledgements. The technical assistance of Laura Trice, Tünde Magyar, Yan Yan Chu and Alyssa Zuehl is highly appreciated. We thank Dr Norbert Solymosi for suggestions about data analysis.

Conflict of interest statement. The authors have no conflict of interest.

Role of authors. Study concept and design: LN, AWR. Acquisition of data: LN, RMF, LMC, EP, MA, BJ. Analysis and interpretation of data: LN, AWR, RMF, CP. Drafting of the manuscript: LN, RMF, AWR. Statistical analysis: LN, CP. Obtained funding: LN, AWR.

For Peer Review

REFERENCES

Ashaber M, Palfi E, Palmer C, Friedman R, Chen L, Roe A, Negyessy L. 2011. Preferential connections of area 1 fingertip representation in primary somatosensory cortex of squirrel monkey. 13th Conference of the Hungarian Neuroscience Society (MITT). Front Neurosci doi: 10.3389/conf.fnins.2011.84.00083

Bensmaia SJ, Denchev PV, Dammann JF 3rd, Craig JC, Hsiao SS. 2008. The representation of stimulus orientation in the early stages of somatosensory processing. J Neurosci 28:776-786.

Bohlhalter S, Fretz C, Weder B. 2002. Hierarchical versus parallel processing in tactile object recognition: a behavioural-neuroanatomical study of aperceptive tactile agnosia. Brain 125:2537-2548.

Bosking WH, Zhang Y, Schofield B, Fitzpatrick D. 1997. Orientation selectivity and the arrangement of horizontal connections in tree shrew striate cortex. J Neurosci 17:2112-2127.

Burton H, Fabri M. 1995. Ipsilateral intracortical connections of physiologically defined cutaneous representations in areas 3b and 1 of macaque monkeys: projections in the vicinity of the central sulcus. J Comp Neurol 355:508-538.

Buzás P, Kovács K, Ferecskó AS, Budd JM, Eysel UT, Kisvárday ZF. 2006. Model-based analysis of excitatory lateral connections in the visual cortex. J Comp Neurol 499:861-881.

Calford MB. 2002. Dynamic representational plasticity in sensory cortex. Neuroscience 111:709-738.

For Peer Review

Chen LM, Friedman RM, Ramsden BM, LaMotte RH, Roe AW. 2001. Fine-scale organization of SI (area 3b) in the squirrel monkey revealed with intrinsic optical imaging. J Neurophysiol 86:3011-3029.

Chen LM, Friedman RM, Roe AW. 2003. Optical imaging of a tactile illusion in area 3b of the primary somatosensory cortex. Science 302:881-885.

Chen LM, Friedman RM, Roe AW. 2009. Area-specific representation of mechanical nociceptive stimuli within SI cortex of squirrel monkeys. Pain 141:258-268.

Chen LM, Turner GH, Friedman RM, Zhang N, Gore JC, Roe AW, Avison MJ. 2007. High-resolution maps of real and illusory tactile activation in primary somatosensory cortex in individual monkeys with functional magnetic resonance imaging and optical imaging. J Neurosci 27:9181-991.

DiCarlo JJ, Johnson KO, Hsiao SS. 1998. Structure of receptive fields in area 3b of primary somatosensory cortex in the alert monkey. J Neurosci 18:2626-45.

Dijkerman HC, de Haan EH. 2007. Somatosensory processes subserving perception and action. Behav Brain Sci 30:189-201.

Fang PC, Jain N, Kaas JH. 2002. Few intrinsic connections cross the hand-face border of area 3b of New World monkeys. J Comp Neurol 454:310-319.

Favorov O, Whitsel BL. 1988. Spatial organization of the peripheral input to area 1 cell columns. I. The detection of 'segregates'. Brain Research 472:25-42.

Fox K. 2009. Experience-dependent plasticity mechanisms for neural rehabilitation insomatosensory cortex. Philos Trans R Soc Lond B Biol Sci 364:369-381.

Friedman RM, Chen LM, Roe AW. 2004. Modality maps within primate somatosensory cortex. Proc Natl Acad Sci USA 101:12724-12729.

For Peer Review

Friedman RM, Chen LM, Roe AW. 2008. Responses of areas 3b and 1 in anesthetized squirrel monkeys to single- and dual-site stimulation of the digits. J Neurophysiol 100:3185-3196.

Garraghty PE, Florence SL, Kaas JH. 1990. Ablations of areas 3a and 3b of monkey somatosensory cortex abolish cutaneous responsivity in area 1. Brain Res 528:165-169.

Gilbert CD, Li W, Piech V. 2009. Perceptual learning and adult cortical plasticity. J Physiol 587:2743-2751.

Godde B, Ehrhardt J, Braun C. 2003. Behavioral significance of input-dependent plasticity of human somatosensory cortex. Neuroreport 14:543-546.

Huffman KJ, Krubitzer L. 2001. Area 3a: topographic organization and cortical connections in marmoset monkeys. Cereb Cortex 11:849-867.

Iwamura Y. 1998. Hierarchical somatosensory processing. Curr Opin Neurobiol 8:522-528.

Iwamura Y, Tanaka M. 1978. Postcentral neurons in hand region of area 2: their possible role in the form discrimination of tactile objects. Brain Res 150:662-666.

Iwamura Y, Tanaka M, Sakamoto M, Hikosaka O. 1983. Functional subdivisions representing different finger regions in area 3 of the first somatosensory cortex of the conscious monkey. Exp Brain Res 51:315-326.

Iwamura Y, Tanaka M, Sakamoto M, Hikosaka O. 1993. Rostrocaudal gradients in the neuronal receptive field complexity in the finger region of the alert monkey's postcentral gyrus. Exp Brain Res 92:360-368.

Iwamura Y. 2000. Bilateral receptive field neurons and callosal connections in the somatosensory cortex. Philos Trans R Soc Lond B Biol Sci 355:267-273.

Jones EG. 1983. Lack of collateral thalamocortical projections to fields of the first somatic sensory cortex in monkeys. Exp Brain Res 52:375-384.

For Peer Review

Jones EG. 2000. Cortical and subcortical contributions to activity-dependent plasticity in primate somatosensory cortex. Annu Rev Neurosci 23:1-37.

Kaas JH. 2004. Evolution of somatosensory and motor cortex in primates. Anat Rec A Discov Mol Cell Evol Biol 281:1148-1156.

Kappers AM. 2011. Human perception of shape from touch. Philos Trans R Soc Lond B Biol Sci 366:3106-14.

Kaskan PM, Lu HD, Dillenburger BC, Kaas JH, Roe AW. 2009. The organization of orientation-selective, luminance-change and binocular- preference domains in the second (V2) and third (V3) visual areas of New World owl monkeys as revealed by intrinsic signal optical imaging. Cereb Cortex 19:1394-1407.

Kisvárday ZF, Tóth E, Rausch M, Eysel UT. 1997. Orientation-specific relationship between populations of excitatory and inhibitory lateral connections in the visual cortex of the cat. Cereb Cortex 7:605-618.

Krubitzer L, Huffman, KJ, Disbrow E, and Recanzone G. 2004. The organization of area 3a in macaque monkeys. J Comp Neurol 471:97-111.

Krubitzer LA, Kaas JH. 1990. The organization and connections of somatosensory cortex in marmosets. J Neurosci 10:952-974.

LaMotte RH, Mountcastle VB. 1979. Disorders in somesthesis following lesions of parietal lobe. J Neurophysiol 42:400-419.

Levitt JB, Yoshioka T, Lund JS. 1994. Intrinsic cortical connections in macaque visual area V2: evidence for interaction between different functional streams. J Comp Neurol 342:551-570.

Li H, Fukuda M, Tanifuji M, Rockland KS. 2003. Intrinsic collaterals of layer 6 Meynert cells and functional columns in primate V1. Neuroscience 120:1061-1069.

For Peer Review

Lipton ML, Liszewski MC, O'Connell MN, Mills A, Smiley JF, Branch CA, Isler JR, Schroeder CE. 2010. Interactions within the hand representation in primary somatosensory cortex of primates. J Neurosci 30:15895-15903.

Lund JS, Yoshioka T, Levitt JB. 1993. Comparison of intrinsic connectivity indifferent areas of macaque monkey cerebral cortex. Cereb Cortex 3:148-162.

Malach R, Amir Y, Harel M, Grinvald A. 1993. A Relationship between intrinsic connections and functional architecture revealed by optical imaging and in vivo targeted biocytin injections in primate striate cortex. Proc Natl Acad Sci USA 90:10469-10473.

Manger PR, Woods TM, Muñoz A, Jones EG. 1997. Hand/face border as a limiting boundary in the body representation in monkey somatosensory cortex. J Neurosci 17:6338-6351.

Merzenich MM, Nelson RJ, Kaas JH, Stryker MP, Jenkins WM, Zook JM, Cynader MS, Schoppmann A. 1987. Variability in hand surface representations in areas 3b and 1 in adult owl and squirrel monkeys. J Comp Neurol 258:281-296.

Négyessy L, Gál V, Farkas T, Toldi J. 2000. Cross-modal plasticity of the corticothalamic circuits in rats enucleated on the first postnatal day. Eur J Neurosci 12:1654-1668.

Negyessy L, Friedman R, Chen LM, Dillenburger BC, Palmer CT, Jakli B, Cserey G, Roe AW. 2009. Intrinsic and extrinsic connections of fingertip representation in the somatosensory cortex of the squirrel monkey. Neuroscience Meeting, Chicago, IL: Society for Neuroscience, Program No. 656.12.

Negyessy L, Goldman-Rakic PS. 2005. Morphometric characterization of synapses in the primate prefrontal cortex formed by afferents from the mediodorsal thalamic nucleus. Exp Brain Res 164:148-154.

Padberg J, Disbrow E, Krubitzer L. 2005. The organization and connections of anterior and posterior parietal cortex in titi monkeys: do New World monkeys have an area 2? Cereb Cortex 15:1938-1963.

For Peer Review

Pálfi E, Roe AW, Friedman R, Chen LM, Dillenburger BC, Palmer C, Négyessy L. 2010. Overlap of connections of fingertip representations in the somatosensory cortex of the squirrel monkey. IBRO International Workshop, Pécs, Hungary, Front Neurosci doi: 10.3389/conf.fnins.2010.10.00256

Pei YC, Hsiao SS, Craig JC, Bensmaia SJ. 2010. Shape invariant coding of motion direction in somatosensory cortex. PLoS Biol 8: e10000305.

Pons TP, Garraghty PE, Cusick CG, Kaas JH. 1985. The somatotopic organization of area 2 in macaque monkeys. J Comp Neurol 241:445-466.

Pons TP, Kaas JH. 1986. Corticocortical connections of area 2 of somatosensory cortex in macaque monkeys: a correlative anatomical and electrophysiological study. J Comp Neurol 248:313-335.

Powell TP, Mountcastle VB. 1959. Some aspects of the functional organization of the cortex of the postcentral gyrus of the monkey: a correlation of findings obtained in a single unit analysis with cytoarchitecture. Bull Johns Hopkins Hosp 105:133-162.

Ratzlaff EH, Grinvald A. 1991. A tandem-lens epifluorescence macroscope: hundred-fold brightness advantage for wide-field imaging. J Neurosci Methods 36:127-137.

Reed JL, Pouget P, Qi HX, Zhou Z, Bernard MR, Burish MJ, Haitas J, Bonds AB, Kaas JH. 2008. Widespread spatial integration in primary somatosensory cortex. Proc Natl Acad Sci USA 105:10233-10237.

Reed JL, Qi HX, Pouget P, Burish MJ, Bonds AB, Kaas JH. 2010a. Modular processing in the hand representation of primate primary somatosensory cortex coexists with widespread activation. J Neurophysiol 104:3136-3145.

Reed JL, Qi HX, Zhou Z, Bernard MR, Burish MJ, Bonds AB, Kaas JH. 2010b. Response properties of neurons in primary somatosensory cortex of owl monkeys reflect widespread spatiotemporal integration. J Neurophysiol 103:2139-57.

For Peer Review

Rockland KS, Knutson T. 2000. Feedback connections from area MT of the squirrel monkey to areas V1 and V2. J Comp Neurol 425:345-368.

Rockland KS, Knutson T. 2001. Axon collaterals of Meynert cells diverge over large portions of area V1 in the macaque monkey. J Comp Neurol 441:134-147.

Sathian K, Stilla R. 2010. Cross-modal plasticity of tactile perception in blindness. Restor Neurol Neurosci 28:271-281.

Shanks MF, Powell TP. 1981. An electron microscopic study of the termination of thalamocortical fibres in areas 3b, 1 and 2 of the somatic sensory cortex in the monkey. Brain Res 218:35-47.

Sincich LC, Blasdel GG. 2001. Oriented axon projections in primary visual cortex of the monkey. J Neurosci 21:4416-4426.

Sterr A, Müller MM, Elbert T, Rockstroh B, Pantev C, Taub E. 1998. Perceptual correlates of changes in cortical representation of fingers in blind multifinger Braille readers. J Neurosci 18:4417-4423.

Sur M, Garraghty PE, Bruce CJ. 1985. Somatosensory cortex in macaque monkeys: laminar differences in receptive field size in areas 3b and 1. Brain Res 342:391-395.

Sur M, Merzenich MM, Kaas JH. 1980. Magnification, receptive-field area, and "hypercolumn" size in areas 3b and 1 of somatosensory cortex in owl monkeys. J Neurophysiol 44:295-311.

Sur M, Nelson RJ, Kaas JH. 1982. Representations of the body surface in cortical areas 3b and 1 of squirrel monkeys: comparisons with other primates. J Comp Neurol 211:177-192.

Thakur PH, Fitzgerald PJ, Hsiao SS. 2012. Second-order receptive fields reveal multidigit interactions in area 3b of the macaque monkey. J Neurophysiol 108:243-262.

For Peer Review

Tommerdahl M, Delemos KA, Vierck CJ Jr, Favorov OV, Whitsel BL. 1996. Anterior parietal cortical response to tactile and skin-heating stimuli applied to the same skin site. J Neurophysiol 75:2662-2770.

Tommerdahl M, Favorov O, Whitsel BL, Nakhle B, Gonchar YA. 1993. Minicolumnar activation patterns in cat and monkey SI cortex. Cereb Cortex 3:399-411.

Tremblay F, Ageranioti-Bélanger SA, Chapman CE. 1996. Cortical mechanisms underlying tactile discrimination in the monkey. I. Role of primary somatosensory cortex in passive texture discrimination. J Neurophysiol 76:3382-3403.

Ts'o DY, Gilbert CD. 1988. The organization of chromatic and spatial interactions in the primate striate cortex. J Neurosci 8:1712-1727.

Ts'o DY, Roe AW, Gilbert CD. 2001. A hierarchy of the functional organization for color, form and disparity in primate visual area V2. Vision Res. 41:1333-1349.

Vallbo AB, Johansson RS. 1984. Properties of cutaneous mechanoreceptors in the human hand related to touch sensation. Hum Neurobiol 3:3-14.

Weinstein S. 1968. Intensive and extensive aspects of tactile sensitivity as a function of body part, sex and laterality. In: Kenshalo DR, editor. The Skin Senses. Springfield: Thomas Books. p 1995-2218.

Wolters A, Schmidt A, Schramm A, Zeller D, Naumann M, Kunesch E, Benecke R, Reiners K, Classen J. 2005. Timing-dependent plasticity in human primary somatosensory cortex. J Physiol 565:1039-1052.

For Peer Review

Table 1. Summary of the parameters and morphological appearance of the BDA injections in the three cases M, V and J. Values are given in µm. Size of the glass capillary was measured after the injection. Tip diameter represents the inner or outer diameter of the glass capillary used for the BDA injection. Outer diameter was measured if inner diameter was not visible due to minor blood infusion. Therefore, in cases V and J the approximate inner diameter is given in parenthesis. Injection depth was measured from the pial surface by a micromanipulator. Core diameter was measured in the section of the series where it exhibited the largest extent. Core depth: approximate depth of the largest core diameter in the section series. Difference between injection and core depth could result from pulsation and swelling of the brain during the injection. Core layer: approximate cortical depth where the core of the injection was most pronounced in the series of sections. In case V, where the core could not be unequivocally identified (for explanation see the text), the values were derived by measuring the highest density region of diffuse labeling around the electrode track. Track length: the approximate maximum depth where the electrode track could be recognized in the section series. While the electrode track was easy to follow in case V, it was hardly visible in cases M and J.

	Tip diameter	Injection depth	Core diameter	Core depth	Core layer	Track length
M	12 (inner)	350	260	260	260	520
V	30 (outer) (~20 inner)	350	380	390	390	520
J	25 (outer) (~15-17 inner)	350	330	390	260-390	520

For Peer Review

Table 2. Statistical comparisons of the densities of bouton-like structures in selected regions of the three cases. P-values of Student t-test statistics are shown. Significant differences are highlighted by italic. P: terminal-like patches, F: long range fiber tracks, CF: regions without BDA labeled fibers, patches and cell bodies.

	P vs. CF	P vs. F	F vs. CF
M	*0.002*	*0.003*	0.42
V	*0.03*	0.13	0.35
J	*2.8E-06*	*0.0001*	0.16

For Peer Review

CAPTION TO FIGURES

Figure 1. Mapping of digit region in SI with optical imaging and electrophysiology (case M). (A-C) Optical images of squirrel monkey somatosensory cortex in response to stimulation of D4 proximal (A), D4 middle (B), and D4 distal (C) finger pads. Consistent with somatosensory topography, the proximal-to-distal activations move away from the border between areas 3b and 1. Images are taken from the area in the blue frame on D. (D) Electrophysiological mapping from case M. t: tip, m: middle, p: proximal, thn: thenar, hyp: hypothenar, jt: joint, dp: deep, b: base. Yellow dot: BDA injection site. Red and black dotted lines: estimate of areal borders. Although border between areas 1 and 2 is uncertain, it is likely that several of the most posterior recording sites fall within area 2. Axis: m = medial, p = posterior. Scale bars: 1 mm.

Figure 2. Alignment of functional maps and BDA label (case M). (A) Vessel map. Color dots: some of electrophysiological recording sites (see Fig. 1 for full map). Open circles: surface vessel endings used for alignment. Blue arrow: injection site. m: medial, p: posterior. (B) Optical map: blank condition. (C) Optical map in response to D2 tip stimulation reveals one activation in area 3b and another in area 1 (white arrows). (D) Dark field photomicrographs of the resulting label near the BDA injection site aligned and superimposed on the surface vessel map. The figure was made by the superposition of the reconstructed series of this case (6 inverse photomicrographs on each other) with the image of the cortical surface. Green and red circles outline several vessel lumens used for the alignment. (E) Histological section revealing darkly stained injection site and other patches. Open circles: same as those shown in A and D and used to align with vessel lumen across sections. Note the

For Peer Review

almost perfect match of these blood vessels on the serial sections. Break at top of section: end of the central sulcus. (F) Map of BDA-labeled cells projected on cortical surface and some of electrophysiological map. . (G) Enlarged view of the area outlined by the dotted rectangle in (E). Retrogradely labeled neurons appear as small black dots. Patches of darkly stained regions also include the fine net of BDA labeled neuronal processes composed both of dendrites and axons. Arrows show blood vessel cross sections encircled on (E). Arrowheads indicate blood vessels, which are encircled by green near the injection site in (D). White arrows point onto electrode penetrations shown in (F) near d4t and d4ap, respectively. Axis: m = medial, p = posterior. Scale bars represent 1 mm.

Figure 3. Injection sites, finger representations and the demarcation of areal borders in SI. (A-C) Black outlines encompass the representation the distal finger pad based on intrinsic signal optical imaging maps (black outlines) for the 3 cases. Dotted lines mark borders between the somatosensory cortical areas 3b and 1. (D-F) Photomicrographs of the injections site (inverse images) are superimposed on the cortical surface where the stimulus related intrinsic signal obtained by the stimulation of the distal finger pads is outlined. Location of BDA injection site (small circle with white core) within the distal D2 finger pad representation (black outlines). Size of injection is indicated by the dotted outline. Scale bars represent 1 mm on A-C and 250 μm on D-F.

Figure 4. High power, dark field views of the BDA injection sites in the three cases. (A-C) The extension of the highest density labeling representing the uptake zone ranges in about 250-300 μm. Arrows point to retrogradely labeled neurons. Note the high density of labeling at the core of the injection site in cases J (B) and M (C) after 10 and 14 days survival, respectively. High density, diffuse labeling characteristic to the core was absent in case V (A)

For Peer Review

with 20 days survival after the BDA injection. Note also the presence of some damage as a probable consequence of injuring the blood vessels situated in the electrode track of V (arrowhead). The damage probably led to the decreased transport laterally in a sub-region around the injection site (white asterisk). Scale bars represent 250 μm.

Figure 5. Retrograde and anterograde BDA labeling. (A) Retrogradely labeled pyramidal cell. Note the spiny dendritic appendages. (B) Difference of fine axonal (*arrows*) and spiny dendritic processes (arrowhead) is shown (see description in the text). (C) Low resolution image shows the manual demarcation of an anterogradely labeled terminal patch (*pale contour*). (D) Higher magnification shows the appearance of numerous thin fibers and bouton-like structures within another example of a terminal patch. (E) A reversed "Y" shaped, relatively thick, smooth axonal process running between areas 3b and 1. Please note the relatively straight course of this axonal process contrasted to the tortuous running of the axons decorated by bouton-like enlargements as shown on panels (B) and (F). Note also the relatively low magnification of panel (E) compared to that of (B) and (F). (F) Long range, horizontal axonal fibers decorated by bouton-like structures. Arrowhead point to a varicosity giving birth to a bouton with a stalk. Arrows show axonal varicosities. (C-F) are inverse, "dark field" images. Scale bars represent 25 μm.

Figure 6. Horizontal distribution of the retrograde and anterograde BDA labeling in the three different cases (V, J, M). (A-C) Distribution of the retrograde labeling on the merged representations of the serial reconstructions. Small black triangles represent retrogradely labeled neuronal perikarya. Injections site is shown by the white dot. (D-F) Voronoi tessellation as a measure of the density of cell body labeling overlaid on the cortical surface. Voronoi areas are greyscaled providing darker tones for smaller areas using log values. White

For Peer Review

region directly around the injection site, representing about 300 μm, shows the area omitted from the analyses. (G-I) Anterograde labeling is represented by connections intrinsic (blue lines) and extrinsic (red lines) to the hand representation region of area 3b; intrinsic connections mostly course medially and laterally (blue lines) and inter-areal axonal fibers course anteriorly and posteriorly (red lines). Green outlines represent patches of terminal axon arborizations. Fibers crossing the estimated borders of the hand representation of area 3b were defined as long distance, inter-areal; otherwise fibers localized within the hand representation were considered intrinsic. The large lateral vein crossing area 3b in (E) is a characteristic landmark identifying the hand-face border within area 3b. *Dashed lines*: estimated areal borders. Scale bars on C, F and I represent 1 mm and apply also to A,B,D,E,G,.H.

Figure 7. Correspondence of the input and target preference of the D2 fingertip with the electrophysiologically recorded somatotopy. For each case (A-C), terminal patches (black outlines) are superimposed on the color coded density maps of retrogradely labeled neurons and the electrophysiological recording sites. *Black circles with white cores:* electrophysiological recording sites. *Red ellipsoids:* functional regions of similar digit preference. For identification of the electrophysiological recording sites, please refer to Figure 1 of the main text. *D1-D4*: digits 1-4; *D2t-D4t*: digit tips of fingers 1-4. *Arrow:* site of the BDA injection. Color scale: the density values by 3 units of standard deviation (SD) above and below the average. Rostral (r) is up, medial (m) is on the right. Solid lines: estimated areal borders. Scale bar: 1 mm.

Figure 8. Quantification of patches. (A) Size of the individual terminal patches for areas 3b (dark gray), 1 (light gray), and 3a (white) for each of the three cases (M, V, J). Diameter expressed as the average of Feret maximum and Feret minimum is shown on the y-axis. (B)

For Peer Review

Regional distribution of the number of bouton-like structures in P (patch), F (fiber), and CF (devoid of fibers or cells) regions. Average number of bouton-like structures is shown on the y-axis. Average was obtained from bouton counts from three 50 μm^2 sampled squares located in individual sections. Bars represent the average of the mean values of the three cases. Error bars indicate standard deviations.

Figure 9. Input and target preference of the connections revealed by the BDA injection into D2 overlaid on the representation of the distal finger pads. (A-C) input preference is shown by the correspondence of peak labeling densities with the optical imaging maps (black outlines). Color code is given in units of standard deviation (SD) above and below average. (D-F) Target preference is defined by the localization of terminal patches (red outlines) on the optical imaging maps (black outlines). Conventions are the same as in Figure 7. Scale bars represent 1 mm.

For Peer Review

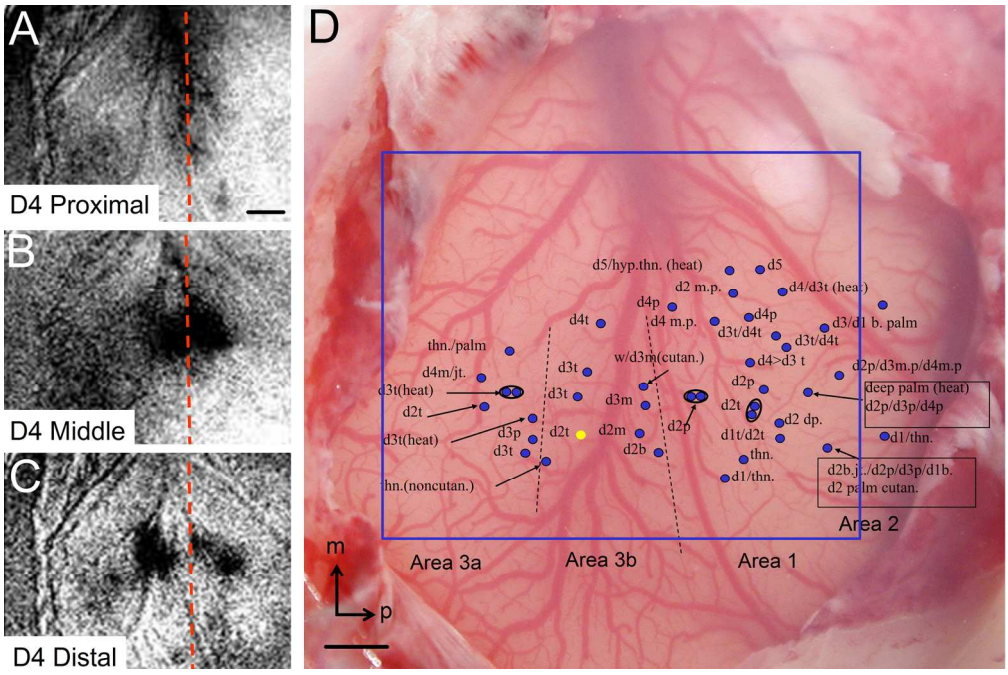


Figure 1. Mapping of digit region in SI with optical imaging and electrophysiology (case M). (A-C) Optical images of squirrel monkey somatosensory cortex in response to stimulation of D4 proximal (A), D4 middle (B), and D4 distal (C) finger pads. Consistent with somatosensory topography, the proximal-to-distal activations move away from the border between areas 3b and 1. Images are taken from the area in the blue frame on D. (D) Electrophysiological mapping from case M. t: tip, m: middle, p: proximal, thn: thenar, hyp: hypothenar, jt: joint, dp: deep, b: base. Yellow dot: BDA injection site. Red and black dotted lines: estimate of areal borders. Although border between areas 1 and 2 is uncertain, it is likely that several of the most posterior recording sites fall within area 2. Axis: m = medial, p = posterior. Scale bars: 1 mm.
169x112mm (300 x 300 DPI)

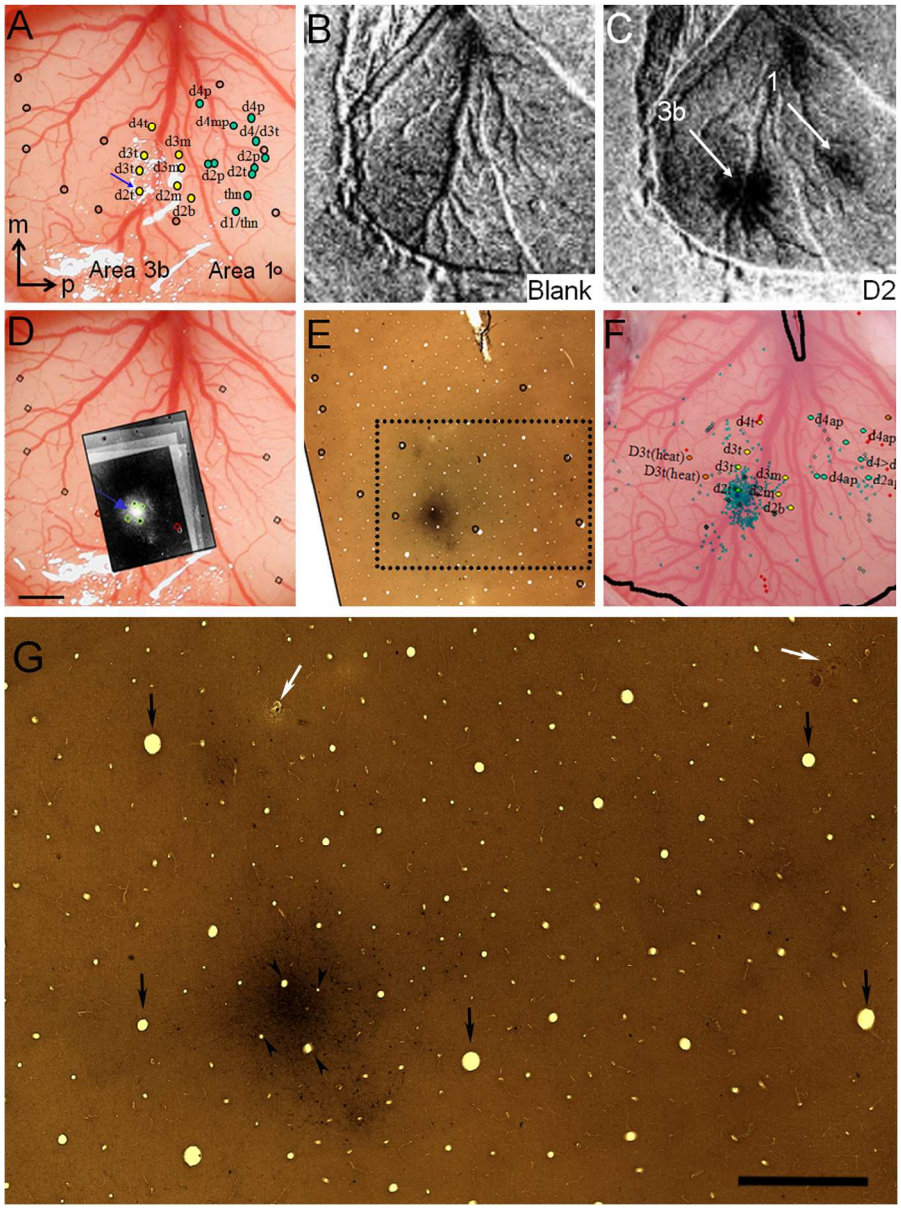


Figure 2. Alignment of functional maps and BDA label (case M). (A) Vessel map. Color dots: some of electrophysiological recording sites (see Fig. 1 for full map). Open circles: surface vessel endings used for alignment. Blue arrow: injection site. m: medial, p: posterior. (B) Optical map: blank condition. (C) Optical map in response to D2 tip stimulation reveals one activation in area 3b and another in area 1 (white arrows). (D) Dark field photomicrographs of the resulting label near the BDA injection site aligned and superimposed on the surface vessel map. The figure was made by the superposition of the reconstructed series of this case (6 inverse photomicrographs on each other) with the image of the cortical surface. Green and red circles outline several vessel lumens used for the alignment. (E) Histological section revealing darkly stained injection site and other patches. Open circles: same as those shown in A and D and used to align with vessel lumen across sections. Note the almost perfect match of these blood vessels on the serial sections. Break at top of section: end of the central sulcus. (F) Map of BDA-labeled cells projected on cortical surface and some of electrophysiological map. . (G) Enlarged view of the area outlined by the dotted rectangle in (E). Retrogradely labeled neurons appear as small black dots. Patches of darkly stained regions

also include the fine net of BDA labeled neuronal processes composed both of dendrites and axons. Arrows show blood vessel cross sections encircled on (E). Arrowheads indicate blood vessels, which are encircled by green near the injection site in (D). White arrows point onto electrode penetrations shown in (F) near d4t and d4ap, respectively. Axis: m = medial, p = posterior. Scale bars represent 1 mm.
169x228mm (300 x 300 DPI)

For Peer Review

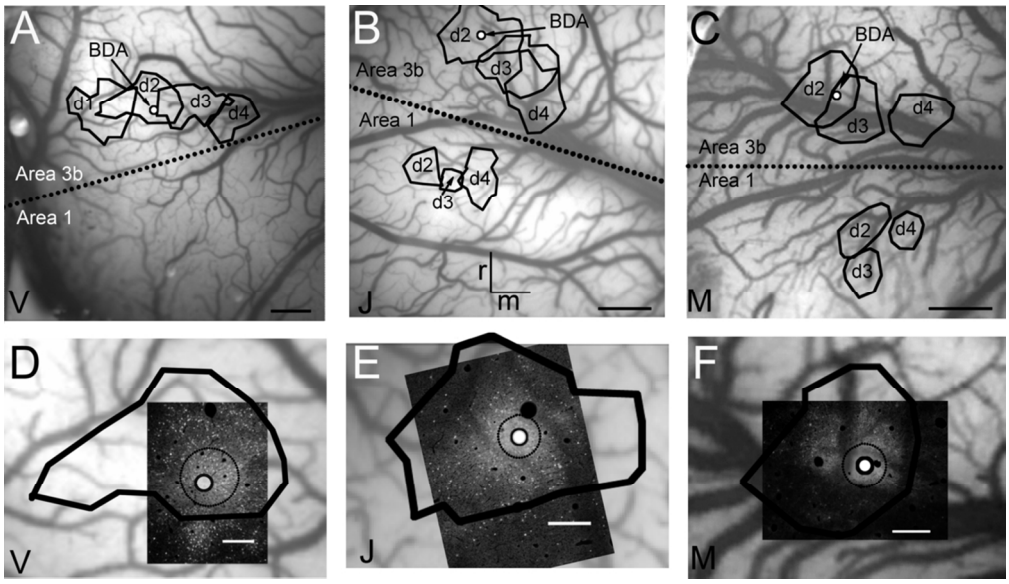


Figure 3. Injection sites, finger representations and the demarcation of areal borders in SI. (A-C) Black outlines encompass the representation the distal finger pad based on intrinsic signal optical imaging maps (black outlines) for the 3 cases. Dotted lines mark borders between the somatosensory cortical areas 3b and 1. (D-F) Photomicrographs of the injections site (inverse images) are superimposed on the cortical surface where the stimulus related intrinsic signal obtained by the stimulation of the distal finger pads is outlined. Location of BDA injection site (small circle with white core) within the distal D2 finger pad representation (black outlines). Size of injection is indicated by the dotted outline. Scale bars represent 1 mm on A-C and 250 µm on D-F.
102x58mm (300 x 300 DPI)

For Review

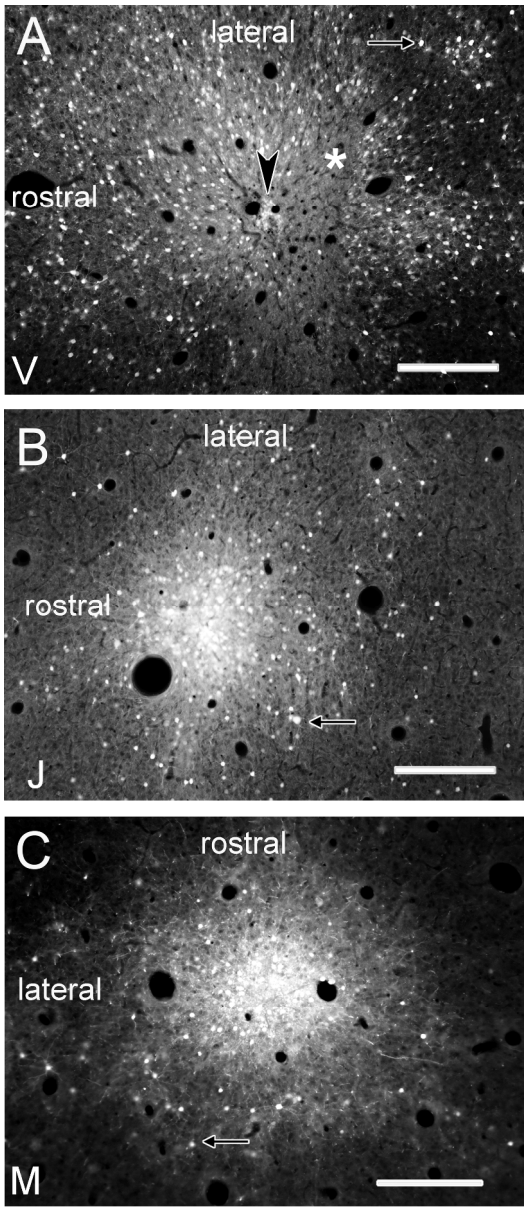


Figure 4. High power, dark field views of the BDA injection sites in the three cases. (A-C) The extension of the highest density labeling representing the uptake zone ranges in about 250-300 μm. Arrows point to retrogradely labeled neurons. Note the high density of labeling at the core of the injection site in cases J (B) and M (C) after 10 and 14 days survival, respectively. High density, diffuse labeling characteristic to the core was absent in case V (A) with 20 days survival after the BDA injection. Note also the presence of some damage as a probable consequence of injuring the blood vessels situated in the electrode track of V (arrowhead). The damage probably led to the decreased transport laterally in a sub-region around the injection site (white asterisk). Scale bars represent 250 μm.
186x431mm (300 x 300 DPI)

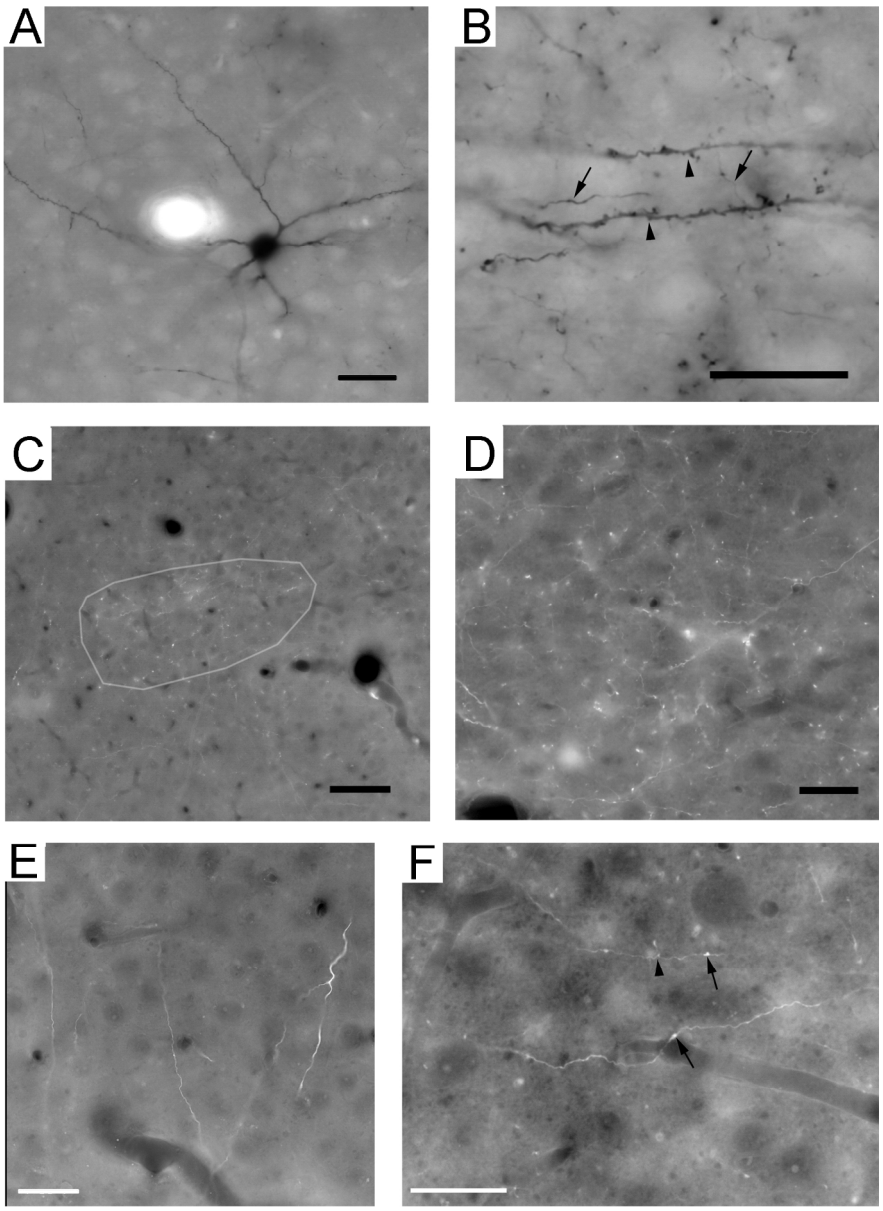


Figure 5. Retrograde and anterograde BDA labeling. (A) Retrogradely labeled pyramidal cell. Note the spiny dendritic appendages. (B) Difference of fine axonal (arrows) and spiny dendritic processes (arrowhead) is shown (see description in the text). (C) Low resolution image shows the manual demarcation of an anterogradely labeled terminal patch (pale contour). (D) Higher magnification shows the appearance of numerous thin fibers and bouton-like structures within another example of a terminal patch. (E) A reversed "Y" shaped, relatively thick, smooth axonal process running between areas 3b and 1. Please note the relatively straight course of this axonal process contrasted to the tortuous running of the axons decorated by bouton-like enlargements as shown on panels (B) and (F). Note also the relatively low magnification of panel (E) compared to that of (B) and (F). (F) Long range, horizontal axonal fibers decorated by bouton-like structures. Arrowhead point to a varicosity giving birth to a bouton with a stalk. Arrows show axonal varicosities. (C-F) are inverse, "dark field" images. Scale bars represent 25 μm.
171x235mm (300 x 300 DPI)

For Peer Review

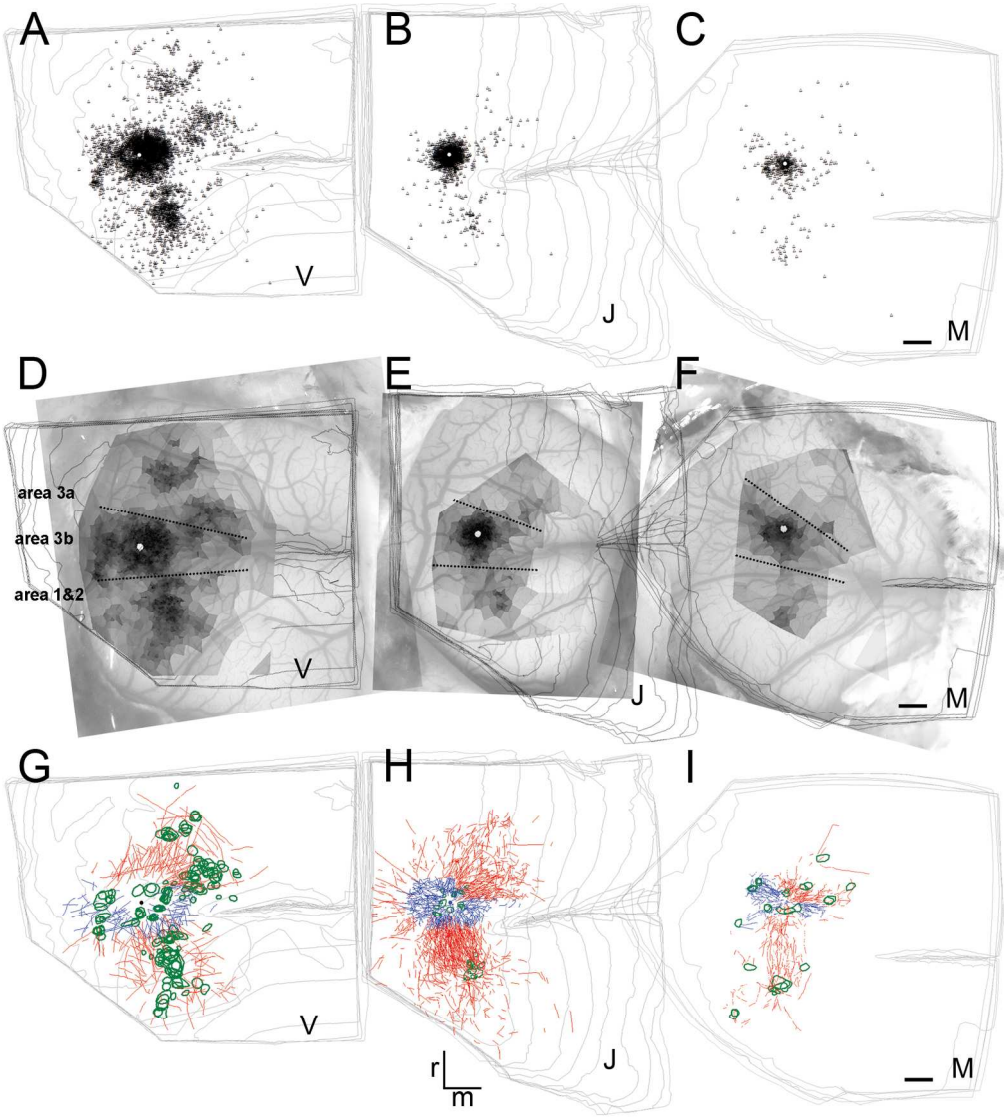


Figure 6. Horizontal distribution of the retrograde and anterograde BDA labeling in the three different cases (V, J, M). (A-C) Distribution of the retrograde labeling on the merged representations of the serial reconstructions. Small black triangles represent retrogradely labeled neuronal perikarya. Injections site is shown by the white dot. (D-F) Voronoi tessellation as a measure of the density of cell body labeling overlaid on the cortical surface. Voronoi areas are greyscaled providing darker tones for smaller areas using log values. White region directly around the injection site, representing about 300 µm, shows the area omitted from the analyses. (G-I) Anterograde labeling is represented by connections intrinsic (blue lines) and extrinsic (red lines) to the hand representation region of area 3b; intrinsic connections mostly course medially and laterally (blue lines) and inter-areal axonal fibers course anteriorly and posteriorly (red lines). Green outlines represent patches of terminal axon arborizations. Fibers crossing the estimated borders of the hand representation of area 3b were defined as long distance, inter-areal; otherwise fibers localized within the hand representation were considered intrinsic. The large lateral vein crossing area 3b in (E) is a characteristic landmark identifying the hand-face border within area 3b. Dashed lines: estimated areal borders. Scale bars on C, F and I represent 1 mm and apply also to A,B,D,E,G,.H.
171x191mm (300 x 300 DPI)

For Peer Review

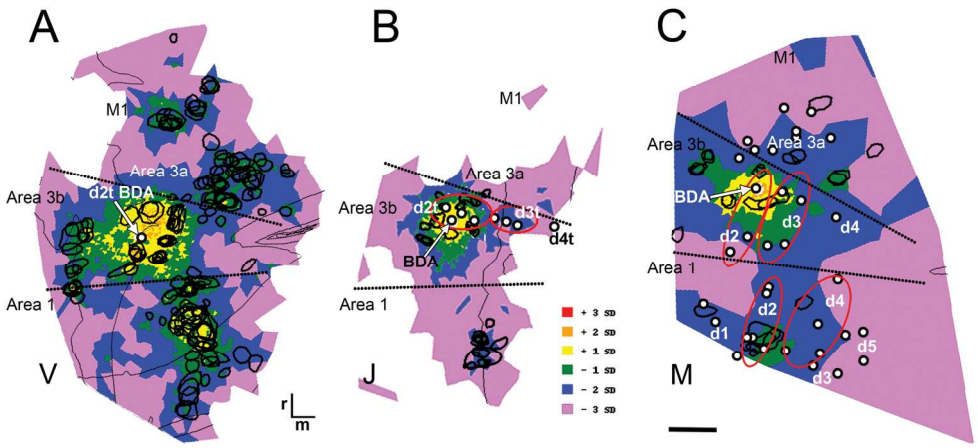


Figure 7. Correspondence of the input and target preference of the D2 fingertip with the electrophysiologically recorded somatotopy. For each case (A-C), terminal patches (black outlines) are superimposed on the color coded density maps of retrogradely labeled neurons and the electrophysiological recording sites. Black circles with white cores: electrophysiological recording sites. Red ellipsoids: functional regions of similar digit preference. For identification of the electrophysiological recording sites, please refer to Figure 1 of the main text. D1-D4: digits 1-4; D2t-D4t: digit tips of fingers 1-4. Arrow: site of the BDA injection. Color scale: the density values by 3 units of standard deviation (SD) above and below the average. Rostral (r) is up, medial (m) is on the right. Solid lines: estimated areal borders. Scale bar: 1 mm.
171x76mm (300 x 300 DPI)

For Review

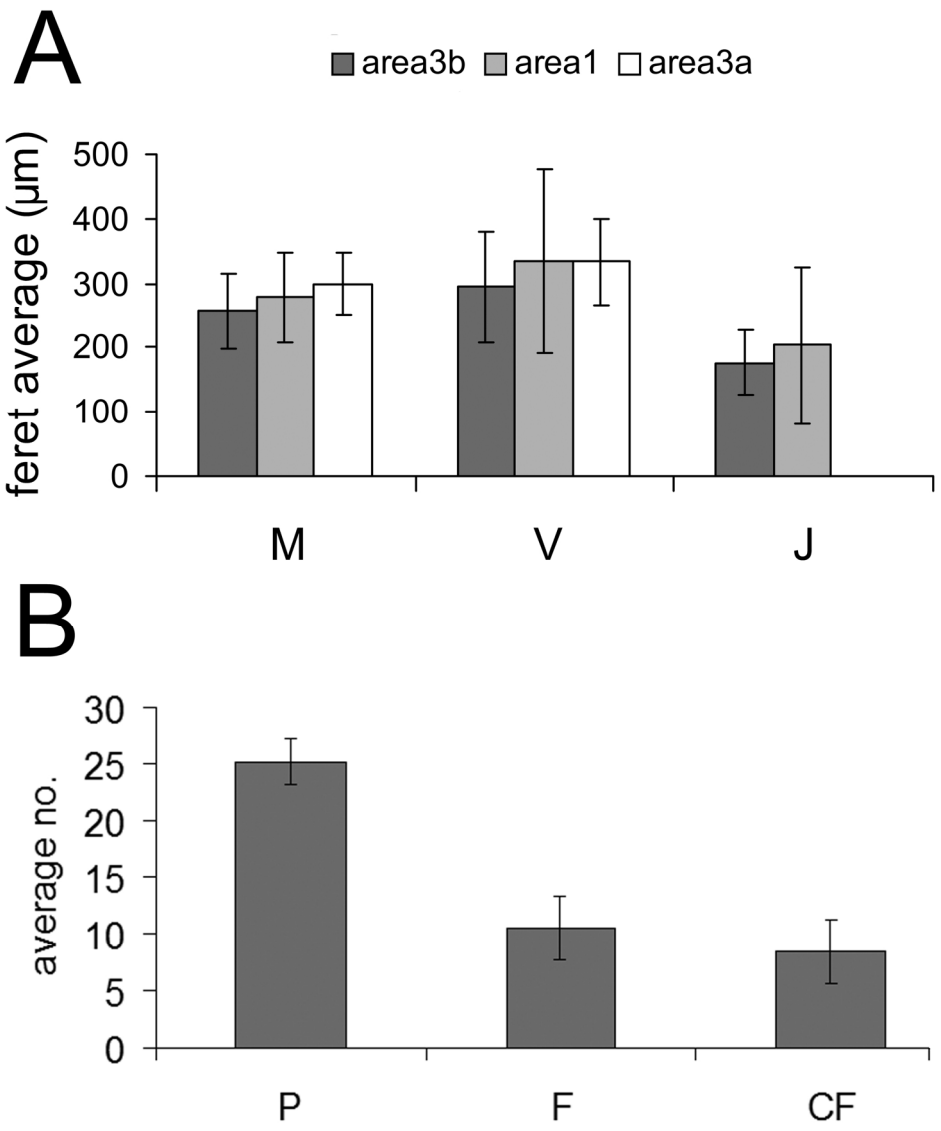


Figure 8. Quantification of patches. (A) Size of the individual terminal patches for areas 3b (dark gray), 1 (light gray), and 3a (white) for each of the three cases (M, V, J). Diameter expressed as the average of Feret maximum and Feret minimum is shown on the y-axis. (B) Regional distribution of the number of bouton-like structures in P (patch), F (fiber), and CF (devoid of fibers or cells) regions. Average number of bouton-like structures is shown on the y-axis. Average was obtained from bouton counts from three 50 µm2 sampled squares located in individual sections. Bars represent the average of the mean values of the three cases. Error bars indicate standard deviations.
94x110mm (600 x 600 DPI)

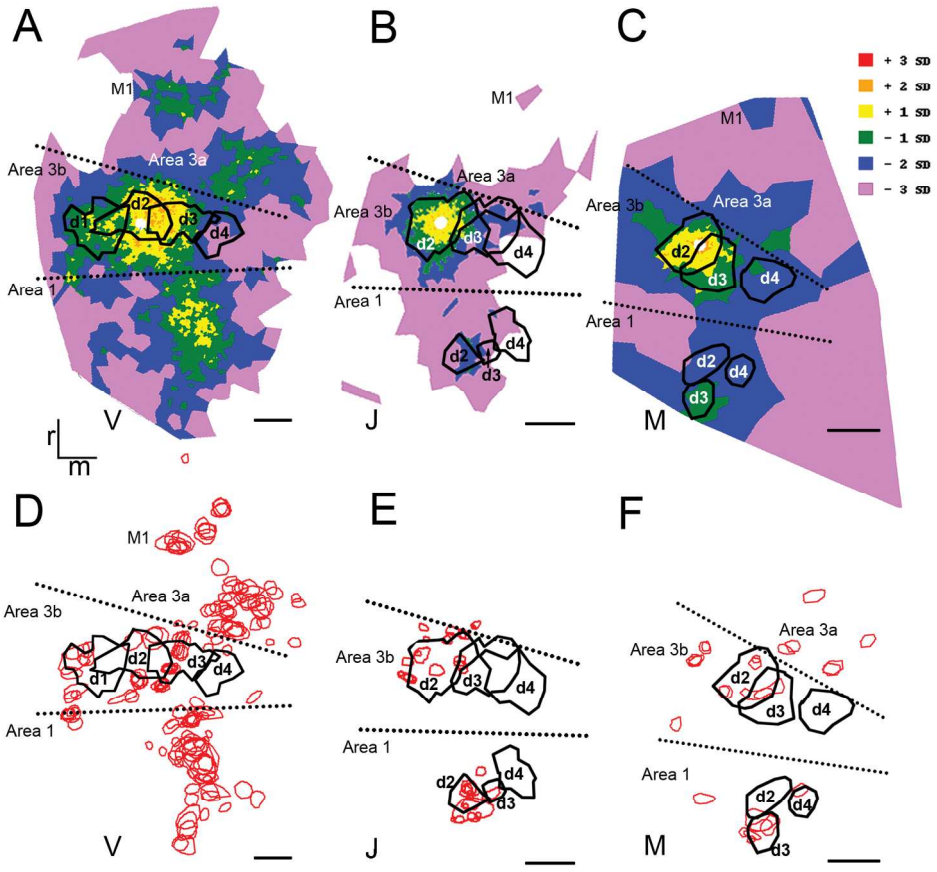
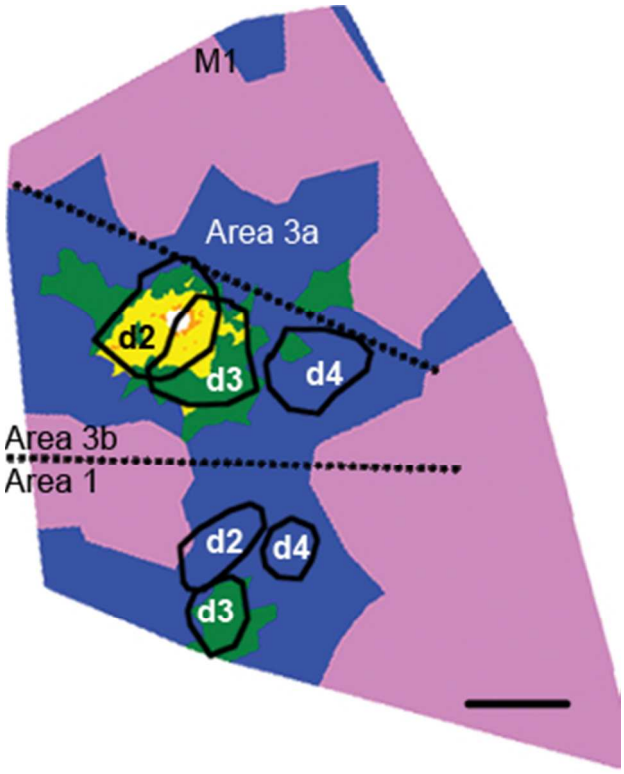


Figure 9. Input and target preference of the connections revealed by the BDA injection into D2 overlaid on the representation of the distal finger pads. (A-C) input preference is shown by the correspondence of peak labeling densities with the optical imaging maps (black outlines). Color code is given in units of standard deviation (SD) above and below average. (D-F) Target preference is defined by the localization of terminal patches (red outlines) on the optical imaging maps (black outlines). Conventions are the same as in Figure 7. Scale bars represent 1 mm.
171x158mm (300 x 300 DPI)

Using bidirectional tract tracing combined with intrinsic signal optical imaging, the authors show strong connectivity between neighboring distal finger pad representations in area 3b of the somatosensory cortex of the squirrel monkey. In contrast, inter-areal connections are apparently digit specific. We propose that intra-areal connectivity is heavily involved in interdigit integration, while long-range inter-areal connections may act in a digit-specific manner. Scale bar = 1 mm.

For Peer Review



Using bidirectional tract tracing combined with intrinsic signal optical imaging, the authors show strong connectivity between neighboring distal finger pad representations in area 3b of the somatosensory cortex of the squirrel monkey. In contrast, inter-areal connections are apparently digit specific. We propose that intra-areal connectivity is heavily involved in interdigit integration, while long-range inter-areal connections may act in a digit-specific manner. Scale bar = 1 mm.
108x135mm (72 x 72 DPI)

iew